STRUCTURE-SOLUBILITY RELATIONSHIPS IN FLUORIDE-CONTAINING PHOSPHATE BASED BIOACTIVE GLASSES

By

YAQOOT SHAHARYAR

A thesis submitted to the

Graduate School-New Brunswick

Rutgers, The State University of New Jersey

In partial fulfillment of the requirements

For the degree of

Master of Science

Graduate Program in Chemical and Biochemical Engineering

Written under the direction of

Ashutosh Goel and Charles Roth

And approved by

_____

_____

_____

New Brunswick, New Jersey

MAY, 2015

ABSTRACT OF THE THESIS

Structure-Solubility Relationships in Fluoride-Containing Phosphate Based Bioactive Glasses

By YAQOOT SHAHARYAR

Thesis Director:

Ashutosh Goel and Charles Roth

The dissolution of fluoride-containing bioactive glasses critically affects their biomedical applications. Most commercial fluoride-releasing bioactive glasses have been designed in the soda-lime-silica system. However, their relatively slow chemical dissolution and the adverse effect of fluoride on their bioactivity are stimulating the study of novel biodegradable materials with higher bioactivity, such as biodegradable phosphate-based bioactive glasses, which can be a viable alternative for applications where a fast release of active ions is sought. In order to design new biomaterials with controlled degradability and high bioactivity, it is essential to understand the connection between chemical composition, molecular structure, and solubility in physiological fluids.Accordingly, in this work we have combined the strengths of various experimental techniques with Molecular Dynamics (MD) simulations, to elucidate the impact of fluoride ions on the structure and chemical dissolution of bioactive phosphate glasses in the system: $10Na_2O$ - (45-x) CaO - $45P_2O_5$ - $xCaF_2$, where x varies between 0 – 10 mol.%. NMR and MD data reveal that the medium-range atomic-scale structure of thse glasses is dominated by Q^2

phosphate units followed by Q^1 units, and the MD simulations further show that fluoride tends to associate with network modifier cations to form alkali/alkaline-earth rich ionic aggregates. On a macroscopic scale, we find that incorporating fluoride in phosphate glasses does not affect the rate of apatite formation on the glass surface in simulated body fluid (SBF). However, fluoride has a marked favorable impact on the glass dissolution in deionized water. Similarly, fluoride incorporation in the glasses results in significant weight gain due to adsorption of water (in the form of OH ions). These macroscopic trends are discussed on the basis of the F effect on the atomistic structure of the glasses, such as the F-induced phosphate network re-polymerization, in a first attempt to establish composition-structure-property relationships for these biomaterials.

Acknowledgements

This work won't have been possible without the support of my thesis supervisor, Prof. Ashutosh Goel. It has been an honor to be his graduate student and learn the basics of glass science from him. I would like to convey my sincere gratitude to thanks to Prof. Charlie Roth for the valuable advice, guidance and encouragement through the course of my master's program. I would also like to extend my heartfelt gratitude to Prof. Richard Lehman for all his support and encouragement that made it possible for me to work in Department of Materials Science and Engineering.

The MD simulation and solid state - nuclear magentic resonance (NMR) studies discussed in this work would not have been possible without the support of Dr. Antonio Tilocca (University College of London, UK) and Dr. Randall E Youngman (Corning, NY), respectively.

The members of my research group have contributed immensely to my personal and professional time and growth at Rutgers. I am especially grateful to Eric Wien (Aresty Summer intern) for his assistance in accomplishing the experimental part of this work. My keen appreciation goes to all the technical and administrative staff including Dr. Robert Horvath and Ms. Nahed Assal for their unconditional support.

I gratefully acknowledge the financial support from Rutgers – School of Engineering, Corning Incorporated, and U.S. Department of Energy – Office of River Protection during the course of my thesis work.

Dedicated to my family

List of Figures

Figure		Page
Figure 1	DTA thermographs of glasses F-5 and F-10 at 20 K min^{-1} in air	13
Figure 2	(a) ^{31}P MAS NMR and (b) ^{23}Na MAS NMR spectra for this series of glasses	14
Figure 3	^{23}Na 3QMAS NMR spectrum of F-2.5 glass. Isotropic and MAS projections are shown to the left and top of the two-dimensional plot. Contours belong to spinning sidebands are denoted by ssb. Extraction of δ_{iso} and P_Q from the peak positions are described in the text.	16
Figure 4	Radial distribution functions for pair interactions involving oxygen (bottom panel) and fluorine (top panel)	17
Figure 5	FTIR Spectra of glass powders	20
Figure 6	(a) XRD data, and (b) FTIR spectra of glasses after dissolution in SBF for 1 h	21
Figure 7	Normalized sodium release rate from glass powders (with respect to their CaF_2 content) after 1 hour of dissolution in SBF	24
Figure 8	pH variation of DI water (with time) due to dissolution of glasses	25

Figure 9	Normalized sodium release profile of glasses (a) F-0, (b) F- 2.5, (c) F-5, (d) F-7.5 after soaking in DI water for 1 h	26
Figure 10	Normalized release profiles for sodium, calcium and phosphate from glasses (as a function of CaF2 content) after soaking in DI water for 1 h	27
Figure 11	Weight loss of glass powders (particle size: 300 – 425 µm), as a function of CaF2 content, after soaking for 120 h in citric acid buffer (pH = 3), Tris-HCl (pH = 7.4), and Tris-HCl (pH = 9), respectively. Labels TH and CA refer to Tris-HCl and citric acid buffer	28
Figure 12	FTIR spectra of glass F-5 before and after dissolution in citric acid buffer (pH = 3) and Tris-HCl (pH = 7.4) for 120 h	29
Figure 13	pH variation of SBF (with time) due to dissolution of glasses	36
Figure 14	Normalized (a) phosphate and (b) calcium (c) sodium release rates from glass powders (with respect time) in F-0, F-5 and F-10 in SBF	37
Figure 15	Normalized (a) phosphate and (b) calcium release rates from glass powders (with respect time) in F-0, F-5 and F-10 in DI water	38
Figure 16	Variation of the weight loss behavior with pH of the dissolution medium	39

List of Tables

Table No		Page
Table 1	Composition of the glass samples synthesized in mole %	5
Table 2	Quantitative analysis of the composition of Simulated Body Fluids	9
Table 3	Overview of weight loss data in the three solutions (citric acid, TH-pH 7.4 and TH-pH 9.0)	10
Table 4	Thermal parameters obtained from DTA analysis	13
Table 5	NMR results based on ^{31}P MAS NMR and ^{23}Na 3QMAS NMR spectroscopy. ^{31}P peak areas included all spinning sidebands. ^{23}Na NMR parameters extracted using peak position in the isotropic and MAS dimensions, as described by Amoureaux et al. [40]. ^{23}Na 3QMAS NMR spectrum of F-2.5 glass. Isotropic and MAS projections are shown to the left and top of the two-dimensional plot. Contours belong to spinning sidebands are denoted by ssb. Extraction of δ_{iso} and P_Q from the peak positions are described in the text	15
Table 6	A-B (B-A) coordination numbers, obtained by integrating the relevant rdfs up to the indicated cutoff distance Rc (Å) corresponding to the first rdf minimum	18
Table 7	Q^n distribution determined from the MD models of the three compositions. NC is the corresponding network connectivity	19

Table of Contents

Chapter			Page no.
	Abstract		
	Acknowledgements		
	List of tables		
	List of figures		
	List of publications		
1.	Introduction		1
2.	Experimental procedure		5
	2.1 Glass synthesis		5
	2.2 Structural characterization		6
		2.2.1 Thermal stability	6
		2.2.2 Magic angle spinning - Nuclear magnetic Resonance (MAS-NMR)	6
		2.2.3 Molecular dynamics simulations	7
	2.3 Apatite forming ability of glasses in simulated body fluid (SBF)		8
	2.4 Chemical dissolution of glasses in deionized water		9
	2.5 Physico-chemical degradation of glasses in accordance with ISO-10993-14		9
3.	Results		12
	3.1 Structural characterization of glasses		12
		3.1.1 Glass transition and thermal stability	12
		3.1.2 MAS-NMR results	14
		3.1.3 Analysis of MD simulations	16
	3.2 Apatite forming ability of glasses in SBF		19
	3.3 Dissolution behaviour of glasses in deionized water		25
	3.4 Influence of pH on dissolution behaviour of glasses		27
4.	Discussion of the Results		30
5.	Conclusions and Future Work		34
6.	Supplementary Results		36

6.1 Apatite forming ability of glasses in SBF 36
6.2 Dissolution behaviour of glasses in deionized water 38
6.3 Influence of pH on dissolution behaviour of glasses 39
References 41

Chapter 1
Introduction

Glass has always been at the center stage of some of the most important discoveries or inventions that have led to revolution in various aspects of human life. One of the first major revolutions leading to saving of lives was the optical microscope which was a seminal step towards discovering microscopic life, eventually leading to elimination of many diseases. The second revolution in healthcare has occurred in the last fifty years in the field of bone regeneration and tissue replacement. The introduction of the concept of 'bioactive materials' with the invention of 45S5 Bioglass® in the late 1960s was a paradigm shift in this direction [1]. Recent research indicates that functional ions and other dissolution products from bioactive glasses, when released in the human physiological system in a controlled manner, can be used to activate genes that stimulate the body to repair itself [2]. This discovery has led to the field of third generation bioresorbable materials with potential tissue-engineering applications [3].

Traditionally, phospho-silicate glasses in the soda-lime silica system based on – or – inspired by – 45S5 Bioglass® have been studied for various applications in the fields of orthopedic surgery, dentistry and other hard/soft tissue engineering, as discussed in recent review articles describe the advances in the field of silicate bioactive glasses [4-8]. Although research on these bioactive glasses is still being actively pursued, mainly directed toward understanding the influence of ionic dissolution products from these glasses on gene activation [9-11], silicate glasses, in general, suffer from some inherent problems associated with their slow chemical degradation, often taking a long time – months to years – to completely disappear from the body. This problem is further amplified when functional ions (i.e. strontium, zinc, fluoride, etc.) are incorporated into these glass compositions, which necessarily affects the dissolution rate. For example, zinc and

strontium (even in small amounts, 2 mol.%) are known to slow down the chemical degradation of bioactive glasses [12, 13]. Similarly, fluoride is known as "corrosion inhibitor" in silicate glasses [14] as it tends to increase the polymerization of silicate tetrahedra by removing modifiers from the siliceous matrix [15]. Therefore, non-silicate fully bioresorbable glass systems are being explored as potential third generation biomaterials.

Bioactive glasses designed in the polyphosphate region of the Na_2O-CaO-P_2O_5 system are an ideal example of one such category of bioresorbable materials. In particular, the glass composition system: $(Na_2O)_{55-x}$ $(CaO)_x$ $(P_2O_5)_{45}$ (where x varies between 30 – 45 mol.%) has received considerable attention owing to its favorable attributes such as controlled chemical dissolution, good cyto-compatibility, along with its soluble nature [16-20]. According to Bitar et al. [20], glasses with CaO content lower than 40 mol.% support little or no cell adhesion and survival due to their high solubility which does not allow cell adhesion to the labile glass surface (as has also been shown by Gough et al. [21, 22]). On the other hand, glass compositions with CaO content varying between 40 – 48 mol.% have been shown to up-regulate human osteoblast cell lines and certain antigens, including bone sialoprotein and fibronectin, which plays a major role in the structure and integrity of bone [19, 20]. The present study is focused on understanding the impact of fluoride incorporation on the structure and solubility of bioactive phosphate glasses. Based on the existing literature in this domain, we have chosen a 10 Na_2O – 45 CaO – 45 P_2O_5 (mol. %) composition as a model glass system where CaO has been substituted by CaF_2 in the range of 0 – 10 mol.%.

Fluoride-releasing biomaterials have found wide application in the field of dentistry due to their anticariogenic properties [23], ability to control enamel demineralization [24] and treat dentine hypersensitivity [25]. Today, there are several fluoride-containing dental restoratives available in the market including glass-ionomers and resin modified glass ionomer cements. However, most

of these materials are silicate-based glass systems which suffer from slower chemical degradation, as discussed above. Fluoride-containing phosphate-based glasses, on the other hand, are ideal candidates for applications where controlled-release glasses with faster degradation rates (in comparison to silicate glasses) are required.

It is well established that incorporation of functional ions in bioactive glasses has significant impact on their molecular structure, which in turn affects their chemical degradation. Therefore, it is essential to understand the impact of these functional ions on the structure-property relationships in these glasses in order to elucidate mechanisms that govern their dissolution and bioactivity. For fluoride-containing bioactive glasses, substantial effort has been made to unearth the underlying structural drivers that control their bioactivity. For example, it is well known that the structural role of fluoride in silicate glasses depends mainly on the local environment. In fluorinated silica (SiO_2) glass, fluoride tends to bond to silicon (≡Si-F) to form only SiO_3F tetrahedra, with no evidence for the formation of oxyfluorides [26-28]. In modified silicate glasses, the acidic environment induces greater amount of Si–F bonds while , as has been shown by Hayakawa et al. [29]. Since the overall environment in silicate/phosphosilicate bioactive glasses is basic in nature (due to the presence of Na^+, Ca^{2+}, Mg^{2+}, Sr^{2+}, etc.), fluoride is mainly found associated with alkali/alkaline-earth cations forming ionic aggregates, as shown by Kapoor et al. [10] and Lusvardi et al. [30]. The ability of fluoride ion to strip network-modifying cations from the glass network may force the silicate network to re-polymerize by forming Si–O–Si or Si–O–P bonds (depending on the fluoride and phosphate concentration in the glass), thus increasing the network connectivity and slowing down their chemical dissolution.

In the case of fluorinated phosphate glasses, several studies have focused on describing the structural role of fluoride in alkali phosphate, tin phosphate, and alumino-phosphate glass systems [31-34]. It has been reported that fluoride depolymerizes the chain structure of $NaPO_3$ by

replacing bridging P–O–P bonds with terminal P–F species. In the case of fluoride alumino-phosphate glasses, several authors reported that F is predominantly bonded to Al rather than P [32, 35, 36] and almost no P-F bonds were detected in Na-Al-P-O-F glasses by ^{19}F NMR [37]. Although the results obtained in these studies represent valid reference points for understanding the influence of fluoride on the phosphate glass structure, they cannot be straightforwardly translated to bioactive glass systems due to significant difference in their chemistry (bioactive glasses have high CaO content and are Al_2O_3-free). The influence of fluoride on the structure of phosphate-based bioactive glasses in the system $20Na_2O–30CaO–50P_2O_5$ has been recently investigated using ab-initio Molecular Dynamics (AIMD). [38] . Based on a substantial amount of F–P bonding found in the AIMD models, it was proposed that the glass network could be structurally homogeneous on medium-range length scales. However in this specific case the necessarily small number of fluorine atoms in the ab-initio model, in connection with the slow convergence of the P-F coordination number (discussed below), may interfere with the accurate evaluation of P-F bonding based on the AIMD data alone. Larger MD samples and/or corresponding experimental data are thus needed for a full assessment of the effect of fluoride on the phosphate glass structure.

Chapter 2
Experimental Procedure

2.1 Glass Synthesis

The high-purity powders of $NH_4H_2PO_4$ (99%, Alfa Aesar), Na_2CO_3 (99%, FMC Corp.), $CaCO_3$ (99%, Alfa Aesar), SiO_2 (99%, Alfa Aesar) and CaF_2 (99%, Alfa Aesar) were used to prepare batches. Homogeneous mixtures of batches (~50 g), were melted in pure platinum crucibles (covered with a Pt-Rh lid) at 1100 ºC for 1 h in air. Glass frits were obtained by quenching the melt in cold water followed by drying. The glasses have been labeled in accordance with their respective CaF_2 content, i.e. F–0, F–2.5, F–5, F–7.5, and F–10. The compositions of the samples prepared have been presented in Table 1. Fluoride was incorporated in the system at the expense of Calcium. CaO was progressively replaced with CaF_2 in the intervals of 2.5 mole % ranging from fluoride free glass (pure soda lime phosphate) to 10 mole%. CaF_2. The amorphous nature of glasses was confirmed by X-ray diffraction (XRD) analysis (PANalytical – X'Pert Pro; Cu K_α radiation; 2θ range: 10º–90º; step size: 0.007º s^{-1}). We did try to synthesize a glass with 12.5 mol.% CaF_2 content but did not succeed as the melt was highly prone to phase separation/crystallization, resulting in white colored opaque frit on quenching in cold water. The dried glass frit was crushed in a planetary ball mill (Fritsch PULVERISETTE 6 *classic line*) to obtain glass powders, respectively.

Sample	**Na_2O**	**CaO**	**P_2O_5**	**CaF_2**
F-0	10.0	55.0	45.0	0.0
F-2.5	10.0	52.5	45.0	2.5
F-5	10.0	50.0	45.0	5.0
F-7.5	10.0	47.5	45.0	7.5
F-10	10.0	45.0	45.0	10.0

Table 1 – Composition of the glass samples synthesized in mole %

2.2 Structural Characterization

2.2.1 Thermal stability

The thermal stability of glasses was studied by differential thermal analysis (DTA, STA8000, Perkin Elmer Inc.). The glass powders (particle size < 120 μm) weighing ~50 mg were contained in an alumina pan and scanned in air from 30 ºC to 1000 ºC at a heating rate (β) of 20 K min^{-1}. The glass transition temperature (T_g), onset of crystallization (T_c), peak temperature of crystallization (T_p) and melting temperature (T_m) were obtained from the DTA thermographs of all the glasses. Differential Thermal Analysis is widely used in assessing the thermal parameters of materials. In principle it is very similar to differential scanning calorimetry. In the DTA the material under consideration and a reference (an empty pan in our case) undergo a similar identical thermal cycle. The temperature difference between the sample and the reference is recorded and plotted against time or temperature. Thermal changes in the system can be either exothermic (crystallization) or endothermic (melting). In our case exothermic curves point towards the positive y direction and vice versa for endothermic curves.

2.2.2 Magic angle spinning - Nuclear magnetic Resonance (MAS-NMR)

^{31}P MAS NMR experiments were conducted at 11.7 T (202.3 MHz resonance frequency) using a commercial spectrometer (VNMRs, Agilent) and 3.2 mm MAS NMR probe (Varian/Chemagnetics). Powdered glasses were packed into 3.2 mm zirconia rotors with sample spinning at 20 kHz. Radio frequency pulses (0.6 μs), corresponding to a π/6 tip angle, were used along with a 60 s recycle delay to collect nominally 1000 acquisitions. The ^{31}P MAS NMR spectra were processed with minimal Gaussian line broadening (25-50 Hz) and frequency (shift) referenced to 85% H_3PO_4 at 0 ppm. The spectra were fit with Gaussian lineshapes, using

commercial software (Grams), and all spinning sidebands were accounted for in determining the Q^n speciation.

^{23}Na MAS and triple quantum MAS (3QMAS) NMR experiments were conducted at 16.4 T (185.12 MHz resonance frequency) using a commercial spectrometer (VNMRs, Agilent) and 1.6mm MAS NMR probe (Agilent). Powdered glasses were packed into 1.6 mm zirconia rotors, with MAS spinning frequencies of 30 kHz. Short RF pulses (0.6 μs ≈ π/12 tip angle) to uniformly excite the ^{23}Na resonances, along with a 1 second recycle delay, were used to acquire 1000 transients, which were subsequently processed without apodization and frequency referenced to aqueous NaCl at 0 ppm. ^{23}Na 3QMAS NMR experiments were performed using the hyper-complex shifted-echo pulse sequence [39]. RF pulses were calibrated to provide optimized signal to-noise ratio, resulting in hard pulse widths of 2.6 and 1.0 μs, and a soft z-filter reading pulse of 10 μs. 240 acquisitions were collected for each of 40 t_1 values. These data were processed with 50 Hz apodization in both time domains and referenced to aqueous NaCl at 0 ppm. Average δ_{iso} and C_q values for sodium in these glasses were calculated from the 3QMAS NMR spectra using the procedures described by Amoureux *et al.* [40].

2.2.3 Molecular Dynamics simulations

Classical Molecular Dynamics (MD) simulations with the DL_POLY code [41] were performed to obtain atomic-scale models of the glasses, using a well-established computational framework for modeling bioactive glasses. [10, 42, 43]. The force field employed here is based on the shell-model (SM) potential for bioactive phosphosilicate glasses developed by Tilocca et al. [44-46] where full ionic charges are employed. Oxygen atoms are represented as core-shell units connected by damped harmonic springs; Buckingham terms describe the interactions between oxygen shells (Os) with each other and with P, Na, and Ca, using the potential parameters

previously reported [47]. The additional Buckingham parameters for the interaction of F^- ions with each other and with Os, P, Na and Ca ions were fitted to the crystalline structures of fluoroapatite, difluorophosphoric acid anhydride, NaF, and CaF_2. Finally, a three-body truncated harmonic potential is used to control the intra-tetrahedral Os-P-Os angle within phosphate groups, but no arbitrary constraints (such as P-O-P angle terms) are placed on the inter-tetrahedral structure.

Three compositions (x = 0, 5, 10 in (45-x) CaO-10Na_2O-45P_2O_5-$x$$CaF_2$) were modeled. For each composition, the simulation was started from a completely random initial configuration containing approximately 3000 atoms; the two fluorinated compositions modeled, x=5 and 10, contained 68 and 136 fluorine atoms, respectively. This starting configuration was inserted in a periodic cubic box of ~35 Å side, yielding a density corresponding to the experimental one or, when no experimental data were available, to the one estimated based on the measured effect of CaO→CaF_2 substitution on the density of Na-Ca silicate bioglasses [49]. The system was then heated and equilibrated at 2500 K for 60 ps, and then continuously cooled to room temperature at a cooling rate of 5 K/ps. The latter rate has been recently shown to produce MD models of melt-derived bioactive glasses with a sufficiently accurate medium-range structure [50]. A final 200 ps MD run at room temperature was then performed to produce the reference trajectory employed for the structural analysis reported below.

2.3 Apatite forming ability of glasses in simulated body fluid (SBF)

The apatite forming ability of glasses was investigated by immersion of glass powders (<120 μm) in SBF (0.1 g glass powder in 50 ml SBF solution) at 37 ºC. The quantitative composition of SBF has been presented in Table 2. SBF had an ionic concentration nearly equivalent to human plasma, as discussed by Tas [51]. The powder–SBF mixtures were immediately sealed into

sterilized plastic flasks and were placed in an oven at 37 ºC. The SBF solution was replaced every 48 h and sampling took place at different times varying between 1 h and 5 days. The experiments were performed in duplicate in order to ensure the accuracy of results. The apatite forming ability on glass powders was followed by XRD and Fourier Transform Infrared (FTIR) spectroscopy. The IR spectra were acquired using a universal attenuated total reflectance sensor (FTIR-UATR, Frontier™, Perkin Elmer Inc.; scanning resolution: 4 cm^{-1}, 32 scans for background and samples). The elemental release profile of glasses in SBF during initial 48 h was measured using inductive coupled plasma – optical emission spectroscopy (ICP-OES; Optima 8x series, Perkin Elmer Inc.) while pH evolution in SBF was followed using a pH meter (SevenCompact™ S230, Mettler Toledo Inc.).

Ion	**Concentration**
	$mmol^{-1}$
Na^+	142
K^+	5
Ca^{2+}	2.5
Mg^{2+}	1.5
Cl^-	125
HPO_4^-	1
HCO_3^{2-}	27
SO_4^{2-}	0.5

Table 2 Quantitative analysis of the composition of Simulated Body Fluids

2.4 Chemical dissolution of glasses in deionized water

The chemical dissolution of glass powders (<120 μm) in Type II deionized (DI) water (pH: 5.50) was investigated by immersing 0.1 g glass powder in 50 ml DI water at 37 ºC. The powder–water mixtures were immediately sealed into sterilized plastic flasks and were placed in an oven at 37 ºC. The dissolution experiments were performed in the time duration varying between 1 h to 7 days. All the experiments were performed in duplicate in order to ensure the accuracy of results.

The changes in glass structure pre- and post-dissolution were followed by XRD and FTIR-UATR. The elemental release profile of glasses in DI water was measured using ICP-OES while pH evolution in DI water was followed using a pH meter.

2.5 Physico-chemical degradation of glasses in accordance with ISO-10993-14

The degradation tests were performed according to the standard ISO 10993-14 "Biological evaluation of medical devices – Part 14: Identification and quantification of degradation products from ceramics". The test comprises two parts. The first part of the test deals with investigating the degradation behavior of glasses/ceramics in citric acid buffer solution with pH = 3.0. The choice of citric acid solution has been made since osteoclasts release this acid while an extreme low pH = 3.0 simulates a worst case low-end environment. The second part of the test simulates a more frequently encountered *in vivo* pH (7.4 ± 0.1) and therefore investigates the degradation of glasses/ceramics in freshly prepared Tris-HCl buffered solution. In order to understand the influence of pH on the chemical degradation of glasses, we have also studied the chemical degradation of glasses in Tris-HCl at pH = 9. In accordance with ISO standard, 5 g glass powder with particle size varying between 300 – 425 μm was immersed in 100 ml solution at 37 °C for 120 h. The sampling was done after duration of 120 h where the solid and liquid phases were separated by filtering (0.22 μm, Millex GP, Millipore Corporation, U.S.A). The solid samples were then washed in DI water and dried in an oven to constant weight.

Fluoride Content	Buffer	Original Weight	Weight After Leaching	Difference	SD
		Gram	gram	%	
0	Citric Acid	2.5002	1.472	41.1	0.2250
2.5	Citric Acid	2.5000	1.359	45.7	0.1599
5	Citric Acid	2.4998	1.379	44.8	0.0514
7.5	Citric Acid	2.5002	1.428	42.9	0.0589
10	Citric Acid	2.5001	1.216	51.4	0.1010
0	Tris-HCl (pH 7.4)	2.5000	3.980	-59.2	0.2296
2.5	Tris-HCl (pH 7.4)	2.5000	4.370	-74.8	0.5697
5	Tris-HCl (pH 7.4)	2.4999	4.804	-92.2	0.6703
7.5	Tris-HCl (pH 7.4)	2.4999	5.206	-108.2	0.1642
10	Tris-HCl (pH 7.4)	2.4998	5.321	-112.8	0.5634
0	Tris-HCl (pH 9.0)	2.5002	6.908	-176.3	0.0000
2.5	Tris-HCl (pH 9.0)	2.5001	7.546	-201.8	0.3356
5	Tris-HCl (pH 9.0)	2.4997	7.599	-204.0	0.1701
7.5	Tris-HCl (pH 9.0)	2.4997	7.555	-202.2	0.1767
10	Tris-HCl (pH 9.0)	2.5000	7.535	-201.3	0.0583

Table 3 Overview of weight loss data in the three solutions (citric acid, TH-pH 7.4 and TH-pH 9.0)

Table 3 presents a detailed overview of weight loss data in the three solutions (citric acid, TH-pH 7.4 and TH-pH 9.0). It quantitatively highlights the key impact of solution pH and the effects of fluoride incorporation in the system.

The pH along with elemental release profile of glasses in different buffer solutions was measured. A relative weight loss percentage of glass samples after 120 h of immersion in solutions were calculated from the pre- and post-dissolution weight of glass powders while the structural changes in glasses were followed by XRD and FTIR.

Chapter 3

Results

3.1 Structural characterization of glasses

3.1.1 Glass transition and thermal stability

Figure 1 presents the DTA thermographs of glasses F-0 and F-10 at heating rate of 20 K min^{-1} as the representative scans for the glasses investigated in the present study while Table 4 presents the values of thermal parameters obtained for all the glasses. The glass transition temperature (T_g) remained almost constant (469.5±0.47 ºC) with increasing CaF_2 concentration in glasses from 0 to 7.5 mol.%. The addition of 10 mol% CaF_2 in glass F-10 led to an increase in its T_g to ~480 ºC. The phenomenon of glass transition was followed by onset of crystallization (T_c) that tends to shift gradually towards lower temperatures with increasing CaF_2 content until glass F-7.5. The value of T_c moved towards higher temperature by 10 ºC in glass F-10 (in comparison to glass F-7.5) as is evident from Table 4. The crystallization was represented by a single exothermic curve (following T_c) for glasses with CaF_2 content varying between 0 – 5 mol%. The peak temperature of crystallization (T_{p1}) shifted towards lower temperatures with increasing CaF_2 content in glasses. A broad shoulder could be observed in the crystallization curves of glasses F-7.5 and F-10, thus, splitting the curve in two distinct features (Figure 1) indicating the formation of two-or more crystalline phases in these glasses with increasing fluoride content. In coherence with the trend observed for T_g and T_c, the value of T_{p1} for glass F-10 shifted towards higher temperature in comparison to glass F-7.5 while no such variation was observed in T_{p2} values. The crystallization was followed by a sharp endothermic event (T_m) at 759±1.1 ºC in all the glasses corresponding to melting of crystalline phases.

$$K_H = \frac{T_c - T_g}{T_m - T_c} \quad (1)$$

Hrubý parameter was calculated for all the glasses using Equation 1. According to Hrubý [52], the larger value of K_H implies towards greater stability against crystallization on heating and, presumably, greater vitrifiability on cooling. The values of K_H tend to decrease with increasing CaF_2 content in glasses until 7.5 mol.% indicating the decreasing thermal stability of glasses with fluoride incorporation. A higher K_H value pointing towards higher thermal stability was obtained for glass F-10 (in comparison to F-7.5).

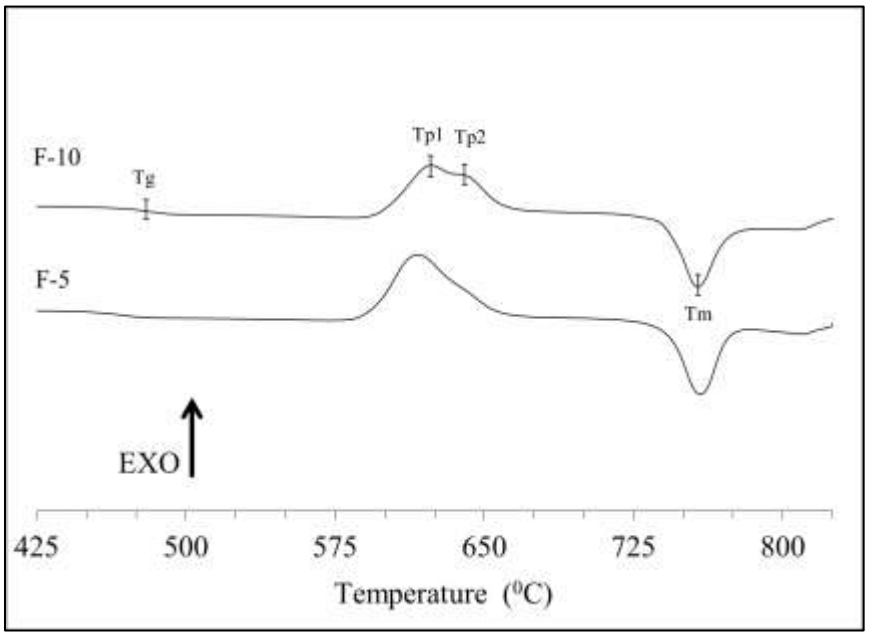


Figure 1 DTA thermographs of glasses F-5 and F-10 at 20 K min^{-1} in air

Glass	T_g	T_{c1}	T_{p1}	T_{p2}	T_m	K_H
F-0	470	608	637	-	760	1.13
F-2.5	470	609	636	-	759	1.12
F-5	469	595	619	-	759	0.90
F-7.5	470	591	611	638	759	0.82
F-10	480	600	623	638	757	0.90

Table 4 Thermal parameters obtained from DTA analysis

3.1.2 MAS-NMR results

Short-range structure in these glasses was investigated with ^{31}P and ^{23}Na NMR spectroscopy. The phosphate speciation, as reflected in the ^{31}P MAS NMR data in Figure 2a, consists entirely of Q^1 and Q^2 polyhedra, corresponding to the resonances at -9 ppm and -25 ppm, respectively. Integration of the peak intensities, including all associated spinning sidebands (not shown), allows for accurately quantification of the phosphate groups (Table 5). The data in Figure 2a, as well as the fitting results in Table 5, indicate little change in phosphate groups with incorporation of CaF_2. The only noticeable difference in Q^1 and Q^2 populations is for glass F-10, which contains a slightly higher fraction of Q^2 groups.

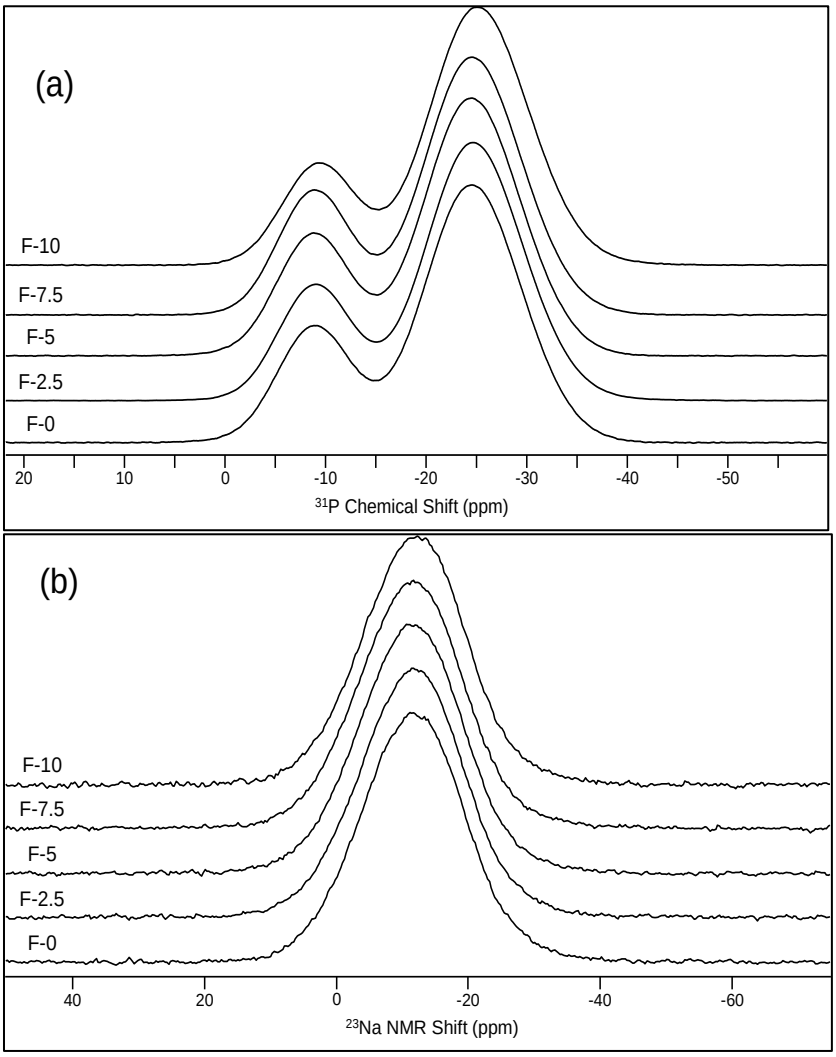


Figure 2 (a) ^{31}P MAS NMR and (b) ^{23}Na MAS NMR spectra for this series of glasses

^{23}Na NMR studies were also made to ascertain the bonding environment of sodium, especially as a function of added fluoride. ^{23}Na MAS NMR spectra are plotted in Figure 2b, showing a single, broad line-shape for all glasses. The position of this resonance under MAS NMR is a combination of both the ^{23}Na chemical shift and a 2nd-order quadrupolar induced shift from the spin-3/2 nucleus. Even without direct determination of the ^{23}Na chemical shifts in these spectra, it is apparent that addition of CaF_2 does not appear to affect the sodium environment in these glasses, as the peaks in Figure 2b are nearly identical for all glasses. ^{23}Na 3QMAS NMR data were also collected to determine chemical shift and quadrupolar coupling values for sodium. The spectra (Figure 3) were analyzed using the position of the ^{23}Na resonance in both frequency dimensions to calculate the ^{23}Na isotropic chemical shift (δ_{iso}) and quadrupolar coupling product (P_Q), using the methods of Amoureaux *et al.* [35] These values are included in Table 5, confirming very little change in either parameter for the sodium in these glasses.

Glass	^{31}P				^{23}Na	
	Q^1		Q^2			
	δ_{CS} (ppm) (± 0.1)	Population (%) (± 1)	δ_{CS} (ppm) (± 0.1)	Population (%) (± 1)	δ_{iso} (ppm) (± 1)	P_Q (MHz) (± 0.2)
F-0	-8.9	22	-24.8	78	-6.2	2.8
F-2.5	-8.9	22	-24.8	78	-5.9	2.8
F-5	-8.8	23	-24.7	77	-6.1	2.7
F-7.5	-8.8	24	-24.7	76	-6.5	2.6
F-10	-9.2	20	-25.3	80	-6.9	2.6

Table 5 NMR results based on ^{31}P MAS NMR and ^{23}Na 3QMAS NMR spectroscopy. ^{31}P peak areas included all spinning sidebands. ^{23}Na NMR parameters extracted using peak position in the isotropic and MAS dimensions, as described by Amoureaux et al. [40]

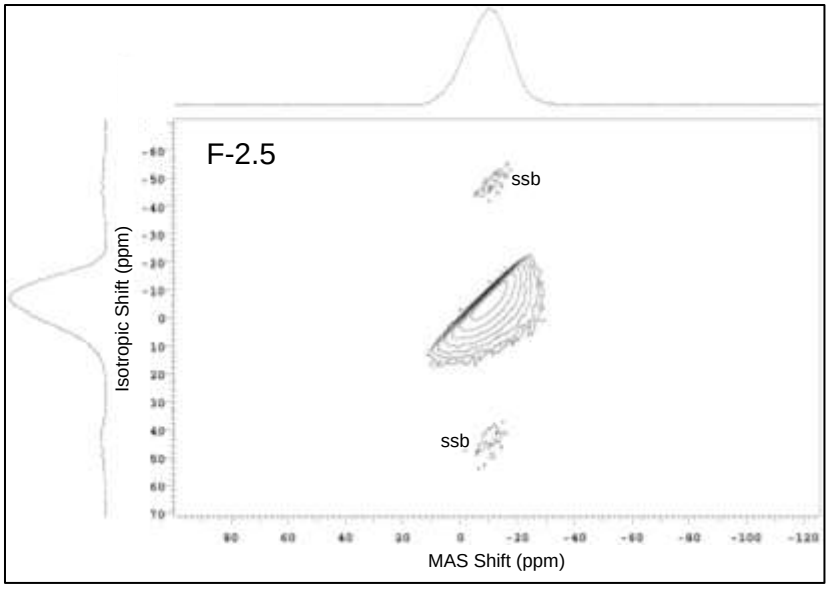


Figure 3
^{23}Na 3QMAS NMR spectrum of F-2.5 glass. Isotropic and MAS projections are shown to the left and top of the two-dimensional plot. Contours belong to spinning sidebands are denoted by ssb. Extraction of δ_{iso} and P_Q from the peak positions are described in the text

3.1.3 Analysis of MD simulations

The radial distribution functions (rdfs) in Figure 4 confirm the accuracy of the force field employed here. The P-O rdf for the F-free composition shows a main peak split into two subpeaks at 1.51 and 1.61 Å, corresponding to P=O and P-O bonds, in agreement with high-energy XRD data for similar compositions [48]. The peaks of the Ca-O, Na-O and O-O rdfs are found at 2.34, 2.37 and 2.56 Å, respectively, also in good agreement with the experimental data. The figure also shows that no marked changes occur in these distances upon CaF_2 incorporation, which therefore does not appear to affect the short-range (local) structure of these glasses. The top panel of the figure shows the rdfs pertaining to fluoride in the two simulated fluorinated compositions. Peaks corresponding to P-F (1.63 Å), Ca-F (2.29 Å), Na-F (2.40 Å), O-F and F-F (2.9-3.0 Å) distances, in absence of relevant experimental data, could be compared to distances measured in previous AIMD simulations of fluorinated phosphate and P-containing bioglasses [38, 53], which yielded corresponding values of 1.58, 2.2-2.25, 2.3 and 3 Å. The agreement is

again rather good, taking into account that the different composition and the corresponding different local environment surrounding fluoride ions are known to markedly affect the F-related distances.[54]

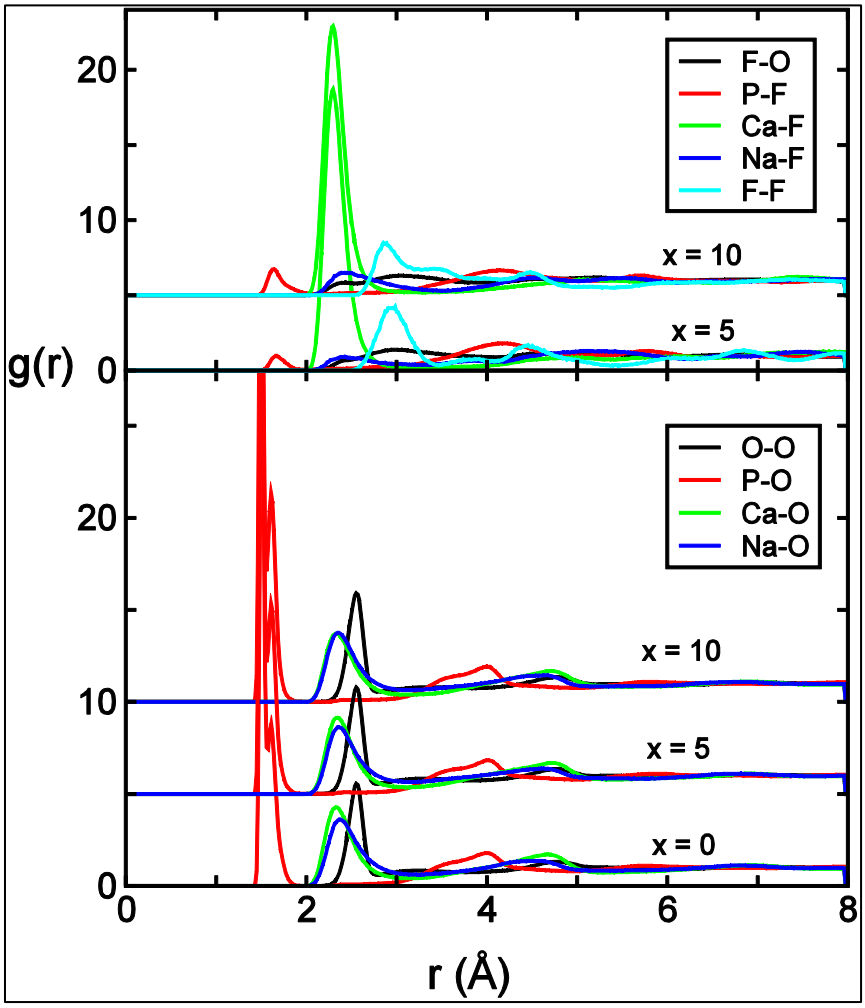


Figure 4 Radial distribution functions for pair interactions involving oxygen (bottom panel) and fluorine (top panel)

Table 6 shows the coordination numbers (CNs) obtained from the MD models. The main message of these data is that, at least up to *x*=10, fluoride is predominantly (although not exclusively) associated to Na and Ca. Only a relatively small amount of fluorine atoms bond to phosphorus, but this P-F bonded fraction appears to increase with increasing CaF_2 fraction: 10% and 20% of all F atoms are bonded to P for *x*=5 and 10, respectively. The total number of (O+F) atoms

bonded to P remains four, indicating that bonding to F does not affect the tetrahedral coordination of phosphorus. It is important to note that the amount of P-F bonding in the melt is initially much higher and only converges slowly to its equilibrium value during the heating/cooling phase. This seems to denote that exceedingly fast cooling rates (relative to the already considerably fast standard values used in MD simulations [50]) may prevent the full convergence of this key property for these systems.

x	**P-O (O-P)**	**P-F (F-P)**	**Na-O (O-Na)**	**Na-F (F-Na)**	**Ca-O (O-Ca)**	**Ca-F (F-Ca)**
	R_c **= 2.0**	R_c **= 2.0**	R_c **= 3.15**	R_c **= 3.35**	R_c **= 3.15**	R_c **= 3.25**
0	4.0 (1.28)	NA	6.68 (1.03)	NA	6.42 (1.47)	NA
5	3.99 (1.30)	0.01 (0.11)	6.27 (0.45)	0.10 (0.21)	5.83 (0.95)	0.61 (2.76)
10	3.96 (1.32)	0.04 (0.20)	6.18 (0.46)	0.3 (0.3)	5.33 (0.89)	1.13 (2.55)

Table 6 A-B (B-A) coordination numbers, obtained by integrating the relevant rdfs up to the indicated cutoff distance Rc (Å) corresponding to the first rdf minimum

Regarding the association to modifier cations, a much higher number of fluoride ions are found in the coordination shell of Ca than Na: this was also evident from the sharp peak in the Ca-F rdfs in Figure 4 as opposed to the much smaller Na-F peak. Table 7 shows the Q^n distribution determined from the MD models of the three compositions. The distribution obtained for the F-free parent composition (F-0) is closer to the NMR data obtained in this work for the same composition, the main difference being the small Q^3 fraction in the model which was not detected by NMR. This distribution is also well compatible with the results previously obtained for related F-free phosphate bioactive glasses using classical MD [55]. The substitution of CaF_2 for CaO leads to a re-polymerization of the phosphate network, as indicated by a decrease in Q^1 and corresponding increase in Q^2 and Q^3 species, reflected in the ~8% increase in network connectivity as x increases from 0 to 10 (Table 7). The NMR data also highlighted a possible network re-polymerization, but only starting for the highest (x=10) CaF_2 fraction, which could be

interpreted based on the loss of fluoride content due to volatilization during melting of the experimental glasses (which does not occur in the simulations) that shifts these trends to higher fluoride contents.

Based on these results, the main effect of fluoride incorporation in these compositions appears to be the removal of modifier cations, especially Ca, from the phosphate network, promoting its re-polymerization. Because the amount of P-F bonding appears to be enhanced with increasing CaF_2 amount, further studies would be needed to understand whether the above re-polymerization effect may change at higher fluoride levels.

x	Q^0	Q^1	Q^2	Q^3	Q^4	*NC*
0	0.08	26.6	68.9	4.4	0	1.78
5	0.58	19.25	73.25	6.9	0	1.87
10	0.61	13.5	77.8	8.0	0.05	1.93

Table 7 Q^n distribution determined from the MD models of the three compositions. NC is the corresponding network connectivity

3.2 Apatite forming ability of glasses in SBF

The FTIR spectra of all the glass powders before immersion in SBF solution are presented in Figure 5. All the investigated glasses show five broad bands in 400–1600 cm^{-1} region. The broadness clearly shows the disorder in the glass structure with uneven distribution of Q^n units (Q is the degree of polymerization and n is the number of bridging oxygens).

The band centered at ~475 cm^{-1} corresponds to the deformation modes of PO_2 units, while the band at 1260 cm^{-1} can be attributed to the asymmetric stretching of PO_2 terminal groups [56]. Similarly, the bands ~750 cm^{-1} and 890 cm^{-1} can be assigned to the symmetric vibrations of bridging oxygens in P–O–P bonds [56] and, asymmetric stretching modes of P–O–P linkages [57],

respectively while, the transmittance band at ~1094 cm^{-1} can be assigned to $P–O^-$ (chain terminator) groups [57].

The immersion of glass powders in SBF for 1 h led to chemical interactions between the two resulting in formation of crystalline phases on the surface of these glasses as is evident from their XRD and FTIR data shown in Figure 6. It should be noted here that the results obtained by soaking of glass powders in SBF for

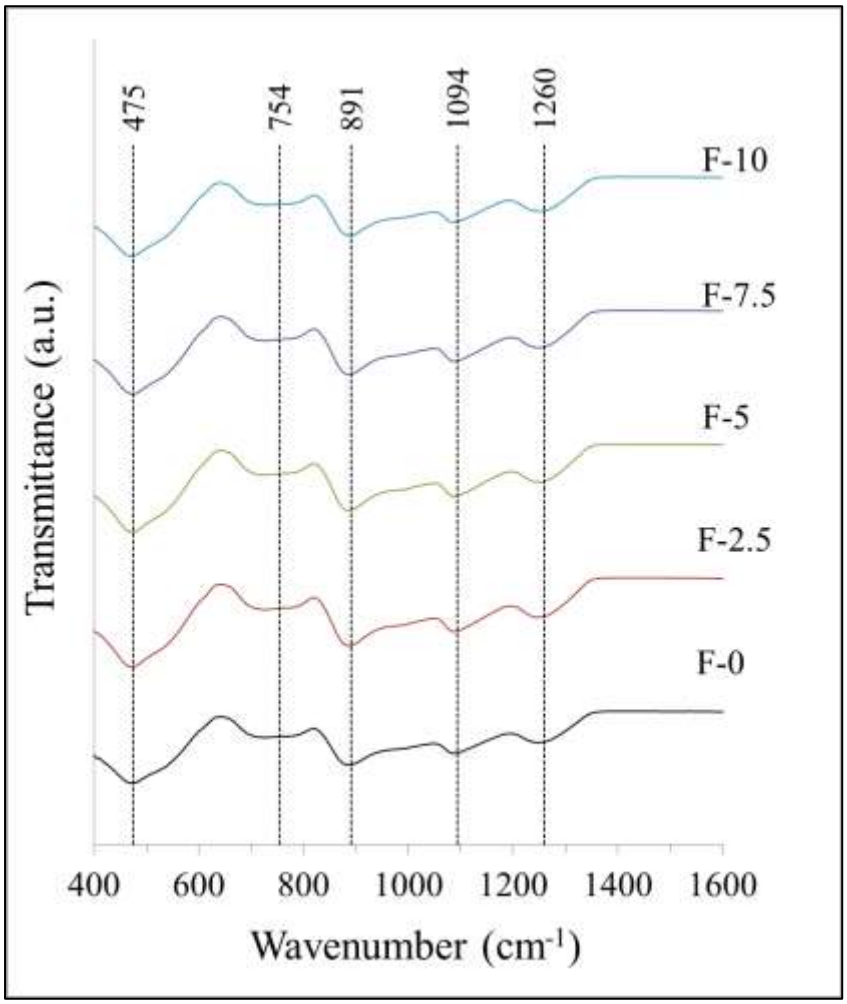


Figure 5 FTIR Spectra of glass powders

prolonged durations were similar to those obtained after 1 h. Therefore, we have focused our analysis and discussion on the results obtained from 1 h of glass – SBF interaction.

The XRD data of glass powders after dissolution in SBF for 1 h demonstrates the formation of calcium phosphate apatite along with aragonite ($CaCO_3$) as shown in Figure 6a. The FTIR spectra of glass powders (Figure 6b) are in good agreement with XRD data as sharp signature bands for calcium phosphate apatite (1040, 1090, 601, and 470 cm^{-1}) and carbonates (1632, 1555, 1462 and 1404 cm^{-1}) [58] can be observed for all the glasses. Our analysis of XRD data yielded three different apatite minerals i.e. stoichiometric hydroxyapatite [$Ca_5(PO_4)_3OH$; PDF#97-005-0656; hereafter referred as HAp], sodium-doped carbonated hydroxyapatite [$Ca_{8.8}Na_{1.2}(PO_4)_{4.8}(CO_3)_{1.2}(CO_3)$; PDF#97-015-3906; hereafter referred as Na-HCA] and fluorapatite [$Ca5(PO_4)_3F$; PDF#97-003-4228; hereafter referred as FAp] as the best possible matches. The possibility of the presence of stoichiometric HAp was negated as the phase reflection corresponding to 100% intensity for this crystal structure appears at $2\theta = 25.85°$ which does not match with our experimental data ($2\theta = 31.85°$, I = 100%). The phase reflections for Na-HCA and FAp demonstrate a good fit with the experimental data. However, the most intense peaks for these phases almost overlap each other at $2\theta = 31.85°$ (Na-HCA) and 31.93 (FAp), thus making it difficult to ascertain the presence of any one phase. In our opinion, the apatite in these glasses comprises a mixture of both Na-HCA and FAp in different proportions where the concentration of FAp increases with increasing fluoride content in glasses. Quantitative phase analysis using Rietveld – RIR method needs to be performed on this data to deduce the exact amounts of phases. Few minor phase reflections ($2\theta = 21.87, 22.81, 26.08, 27.59°$) in these glasses could not be accurately identified (probably some hydrated carbonates) and therefore, have been left unmarked.

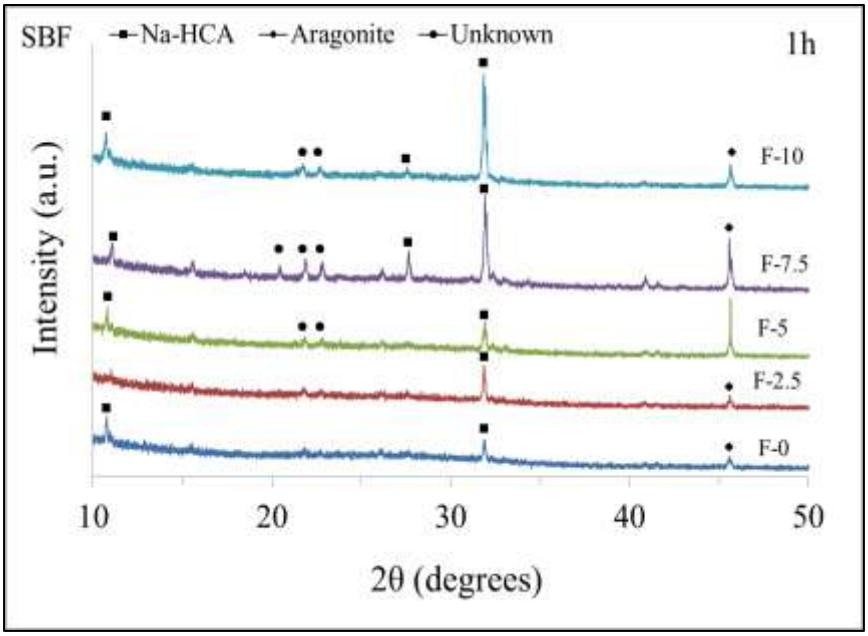


Figure 6 (a) XRD data of glasses after dissolution in SBF for 1 h

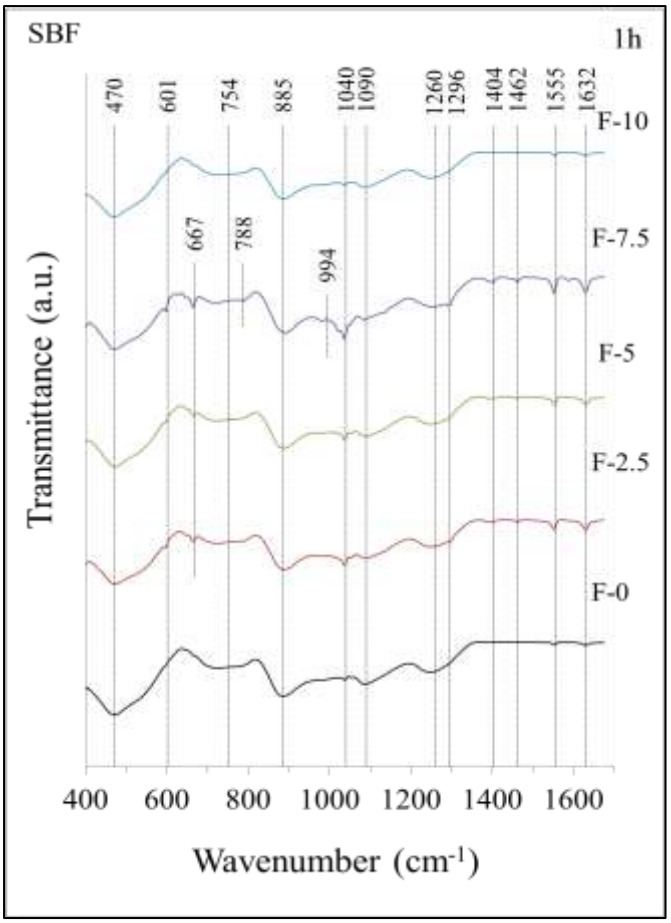


Figure 6 (b) FTIR spectra of glasses after dissolution in SBF for 1 h

With regard to the carbonate substitution in hydroxyapatite, the characteristic FTIR peaks for A-type HCA (hydroxyl is substituted by carbonate group) are known to appear at 880, 1450 and 1540 cm^{-1} while that for B-type HCA (phosphate group is substituted by carbonate group) appear at 870, 1430 and 1450 cm^{-1} [59]. In our study, the characteristic band at ~1550 cm^{-1} has been used to confirm the presence of A-type HCA. The FTIR band at ~1462 cm^{-1} may be attributed to aragonite [60] while 1630 cm^{-1} band represents hydroxyl. Since most of the characteristic IR bands for A-type and B-type HCA tend to overlap each other, it is difficult to negate the possibility of mixture of both A/B-type HCA. According to literature, B-type is the preferential carbonate substitution found in the bone of a variety of species, with A/B type ratio in the range 0.7 – 0.9 [61].

Soda-lime phosphate glasses are known to dissolve congruently in aqueous media through a two-step process: (1) Hydration reaction where the glass exchanges its Na^+ with H^+ ions from the aqueous solution to carry out the formation of a hydrated layer on the glass surface; (2) Network breakage where H^+ ions and molecular water attack the P–O–P bonds in hydrated layer resulting in destruction of the glass network and leading to the release of phosphate chains with different degree of polymerization into the aqueous solution [38, 62-65], a mechanism not dissimilar to that established for silicate bioglasses [47, 66]. Because of the moisture adsorption on the glass surface during its preparation and storage period, P–O–P breakage takes place inside the hydrated layer formed before the dissolution process. Once in contact with SBF, the short chain polyphosphates or orthophosphates quickly dissolve into aqueous solution, leading to rapid increase of phosphate concentration in SBF. On the other hand, while SBF is already calcium and phosphate rich, the affinity of phosphate chains in SBF to chelate with divalent calcium attracts the latter from the hydrated layer of glass into SBF resulting in deposition of apatite and calcium carbonate phases on the glass network structure [62, 65]. The deposition of crystalline phases acts as a protective

film over the hydrated layer preventing further diffusion of molecular water into the bulk glass [62].

When compared with fluorinated silicate bioactive glasses [15, 30, 49, 67-69], we did not find any significant influence of fluoride on apatite forming ability of phosphate-based bioactive glasses as apatite and aragonite phases were observed in all the glasses after 1 h of immersion in SBF and the same crystalline phase assemblage was maintained over the period of 120 h. However, fluoride incorporation in phosphate glasses does affect their initial chemical dissolution (before significant network breakage takes place, Step 2) as can be seen in the normalized sodium release profile of glasses (with respect to CaF_2 content) in SBF after 1 h immersion (Figure 7).

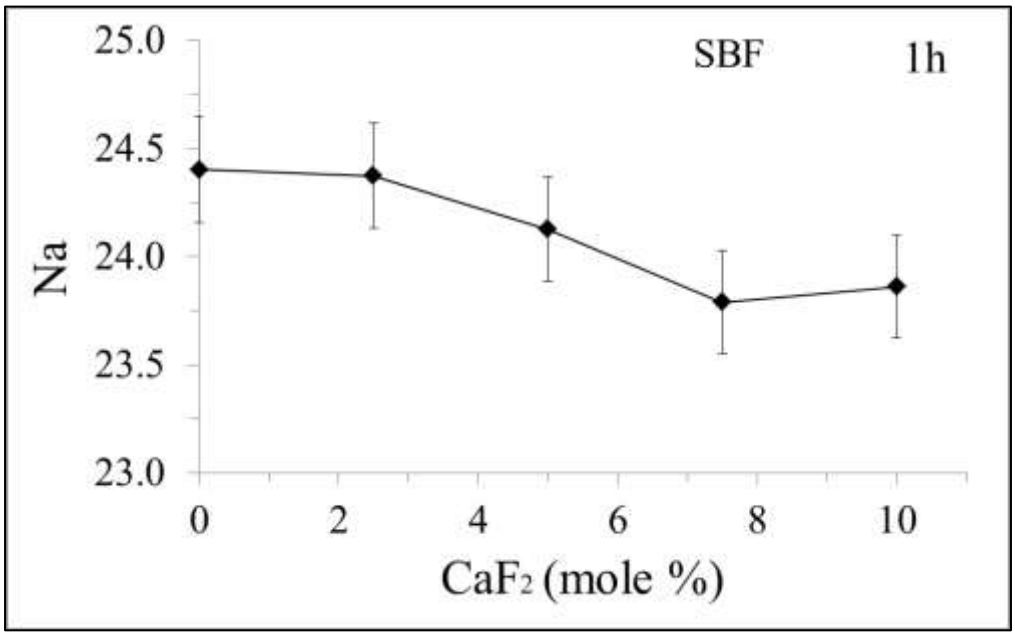


Figure 7 Normalized sodium release rate from glass powders (with respect to their CaF_2 content) after 1 hour of dissolution in SBF

We focused only on the sodium release profile because the dissolution of phosphate glasses is initiated by $Na^+ \leftrightarrow H^+$ ion exchange. The sodium release profile provides vital information concerning the impact of fluoride incorporation on the dissolution behavior of these glasses. It has been shown in literature that $Ca^{2+} \leftrightarrow H^+$ ion exchange reaction does not occur during the formation

of the hydrated layer at the glass–water interface [62]. As is evident from Figure 7, increasing CaF_2 content in glasses led to a slight decrease in their sodium release rate during the first hour of dissolution in SBF. Prolonged duration tests (for example: 48 h) reveal that sodium concentration in SBF was almost the same for all the glasses irrespective of the fluoride content suggesting the dominance of Step 2 (network breakage) in glass dissolution

3.3 Dissolution behavior of glasses in deionized water

The dissolution of glass powders in DI water for durations varying between 1 h – 120 h did not result in any structural changes or formation of crystalline phases on surface of glasses as is evident from FTIR and XRD data (not shown). However, we did obtain some insight into the impact of fluoride on dissolution behavior of phosphate glasses from the elememental release profile of these glasses in DI water. Figure 8 presents the variation in pH of DI water due to dissolution of glasses over the period of 120 h.

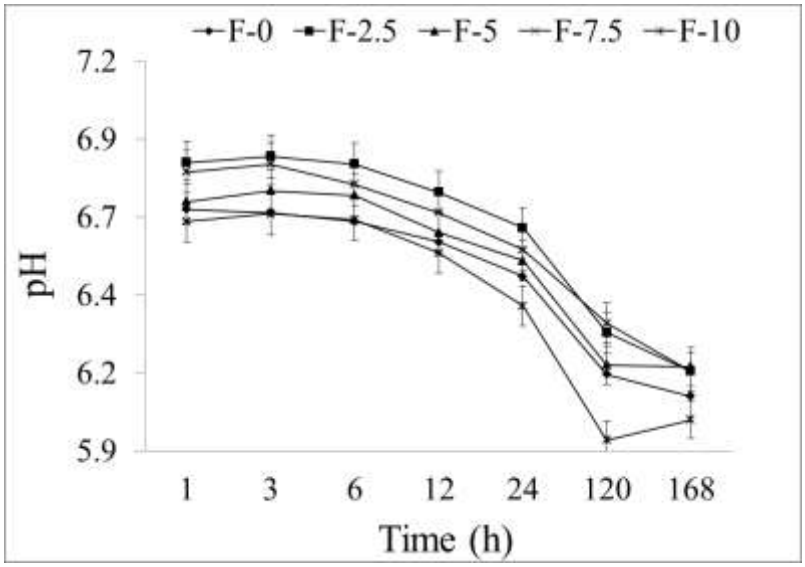


Figure 8 pH variation of DI water (with time) due to dissolution of glasses

As expected, the pH values tend to decrease with increasing glass soaking time indicating breakage of P–O–P bonds between the [PO_4] units under the attack of H^+ ions and molecular water [62]. Since the network breakage reaction is highly sensitive to the attack of H^+ ions, decreasing the pH value of aqueous media can further enhance the dissolution rate of these glasses. Figure 9 presents the normalized sodium release profile of glasses F-0 (Figure 9a), F-2.5 (Figure 9b) and F-5 (Figure 9c) in DI water over the period of 120 h. As is evident from Figure 9a, the CaF_2-free parent glass exhibits forward dissolution rate during initial 3 h after which solution feedback effects could be observed. However, the incorporation of 2.5 mol.% CaF_2 in glasses prolonged the forward dissolution rate of glasses to 24 h (Figure 9b). Further increase in CaF_2 content (>2.5 mol.%) in glasses did not affect the dissolution behavior as can be seen in Figure 9c.

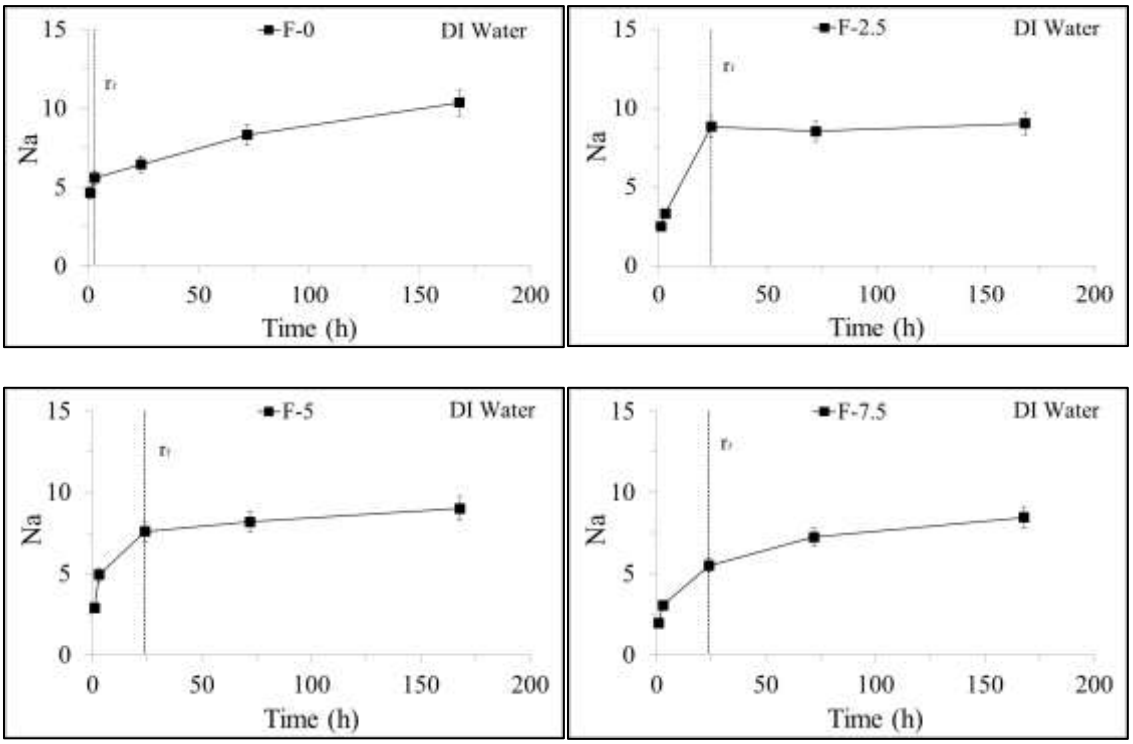


Figure 9 Normalized sodium release profile of glasses (a) F-0, (b) F- 2.5, (c) F-5, (d) F-7.5 after soaking in DI water for 1 h

This increase in duration for forward dissolution rate of glasses from 3 h to 24 h may be attributed to their slower chemical degradation under the influence of fluoride content. Figure 10 presents the normalized release profiles for sodium, calcium and phosphate (as a function of CaF_2 content) from glasses in DI water after soaking for 1 h. As is evident from the ICP-OES data, the elemental release from glasses reduces to half (approximately) due to incorporation of 2.5 mol.% CaF_2. Further increase in CaF_2 content did not exhibit significant influence on the dissolution behavior of glasses. These results are in good agreement with the sodium release profile obtained in SBF (Figure 5) and confirms that fluoride tends to slow down the chemical dissolution of phosphate glasses but only until the stage where glass network structure is not broken by the attack of H^+ and molecular water.

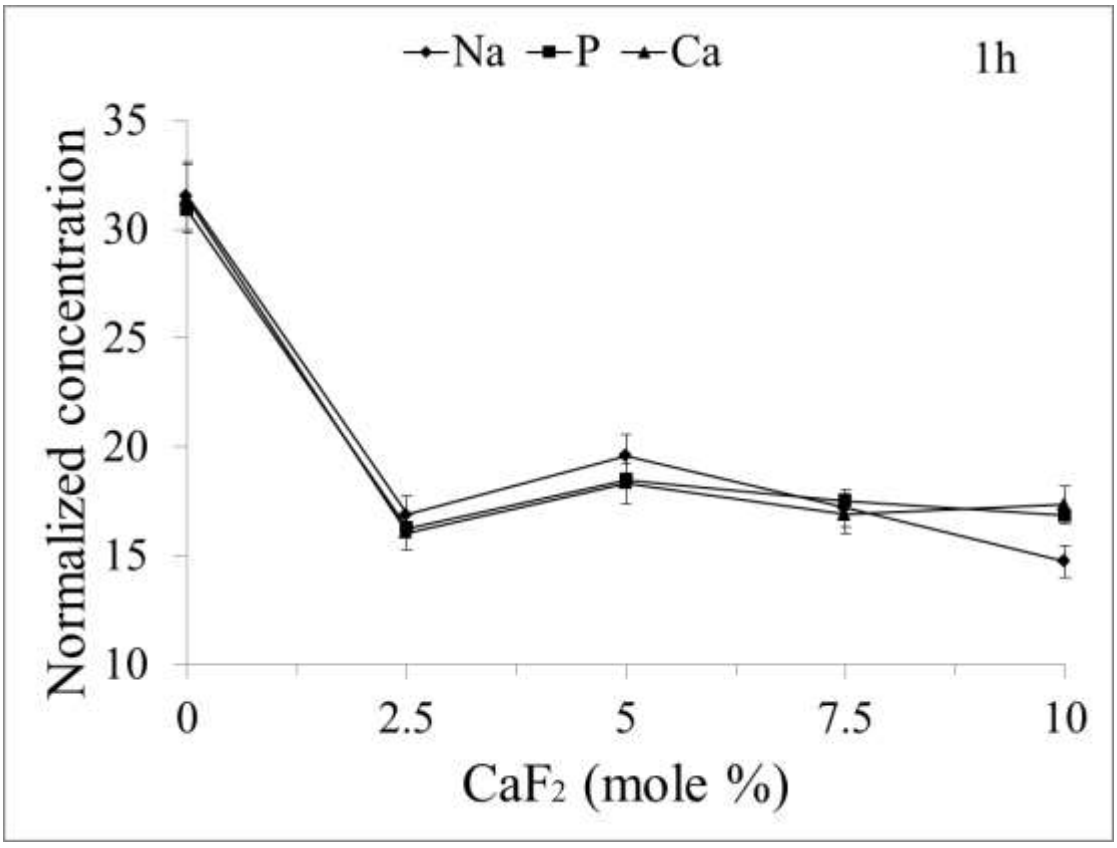


Figure 10 Normalized release profiles for sodium, calcium and phosphate from glasses (as a function of CaF_2 content) after soaking in DI water for 1 h

3.4 Influence of pH on dissolution behavior of glasses

Figure 11 presents the weight loss (%) data of glasses (at different pH) as function of their CaF_2 content. As is evident from the weight loss data, solution pH had a significant impact on the dissolution behavior of glasses. While phosphate glasses showed significant weight loss (40 – 50%) in citric acid buffer (pH = 3) over the period of 5 days, increase in solution pH to 7.4 and 9 resulted in tremendous weight gain in glass powders which increased with increasing solution pH. Fluoride incorporation in glasses did not exhibit any significant impact on the trend of the observed weight loss in acidic media. However, an almost linear relationship was observed between weight gain and fluoride content in glasses at pH = 7.4 and 9, where increasing CaF_2 content in glasses increased their weight gain. FTIR data of glasses (Figure 12) demonstrates high amounts of water uptake in the investigated glasses at neutral and basic pH leading to their negative weight loss.

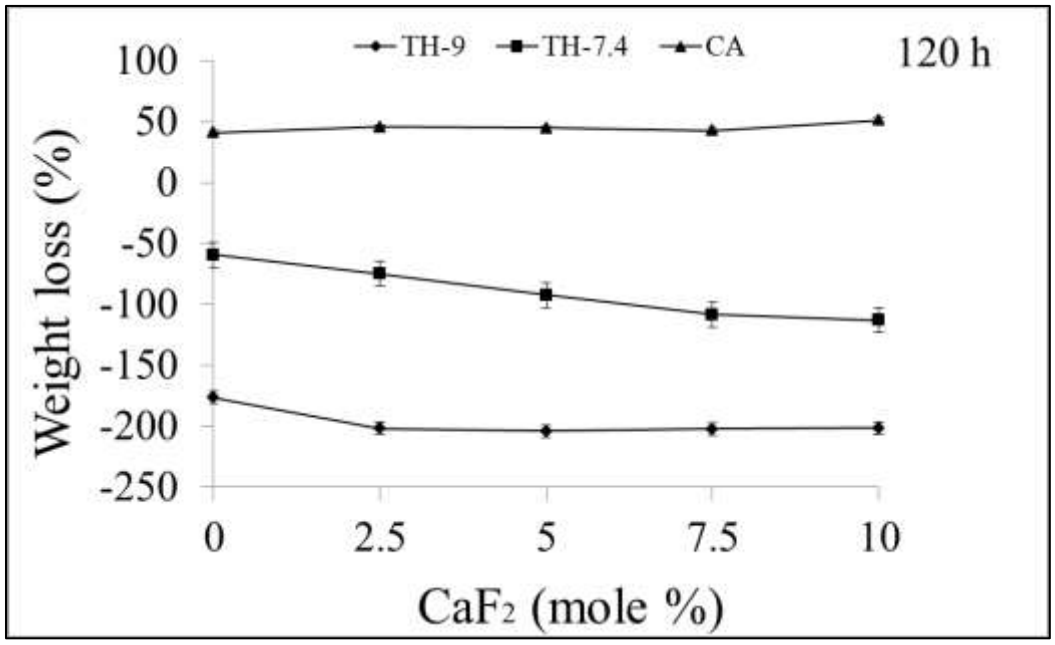


Figure 11 Weight loss of glass powders (particle size: 300 – 425 μm), as a function of CaF_2 content, after soaking for 120 h in citric acid buffer (pH = 3), Tris-HCl (pH = 7.4), and Tris-HCl (pH = 9), respectively. Labels TH and CA refer to Tris-HCl and citric acid buffer

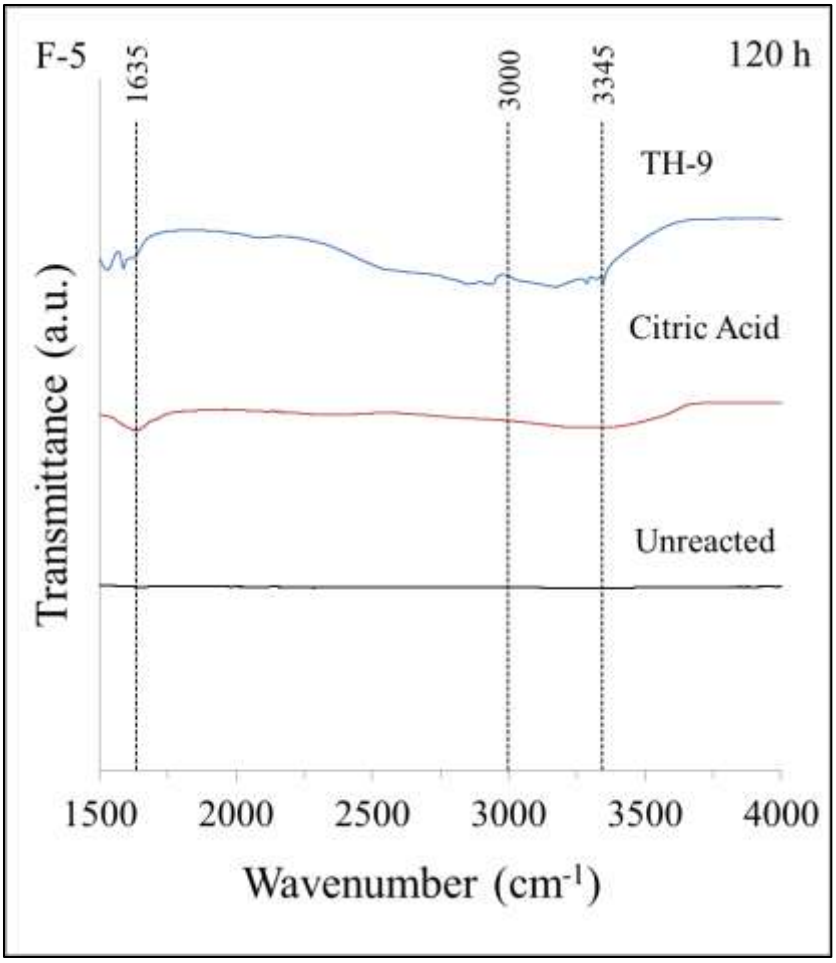


Figure 12 FTIR spectra of glass F-5 before and after dissolution in citric acid buffer (pH = 3) and Tris-HCl (pH = 7.4) for 120 h

Chapter 4

Discussion of the Results

The chemical dissolution of glasses is a complex topic and there is still no complete consensus on the basic mechanism of glass corrosion that applies to a wide composition space. In particular for phosphate-based bioactive glasses, our understanding of their chemical dissolution has advanced from simple composition-dependent models [62, 70-72] to those based on composition-structure-property relationships [65, 73]. This evolution has been driven by the idea that the understanding of relationships between chemical composition of glasses and their structure at atomistic level will help us in unearthing the fundamental mechanisms of glass corrosion. This understanding of structure-property relationships in bioactive glasses is of utmost importance for the development of a new generation of gene-activating bioactive glasses with controlled release of functional ions tailored for the treatment of specific conditions [74]. However, despite the ongoing strenuous effort in this direction, we are still not in a position to develop scientifically robust and statistically accurate models to predict the chemical dissolution behavior of glasses based on their structure-property relationships. This may be attributed to the fact that during dissolution of glasses in aqueous solutions, several chemical processes occur simultaneously within the glass and in solution, so that a rigorous combination of theoretical and experimental studies is required for robust interpretation and reliable predictions of glass corrosion. With this perspective, the present study aims at combining the strengths of experimental and computational studies to elucidate the structural role of fluoride on the chemical dissolution and bioactivity of phoshpate based bioactive glasses.

It is well known that incorporation of modifier cations (Ca^{2+} and Na^{+}) in the phosphate glass network results in the breaking of P-O-P linkages leading to the formation of NBOs, and decrease in the chemical durability of glasses [75]. While the two cations compete to bond with the NBOs present in the network, the coordination of Ca is satisfied preferentially over Na, owing to its higher field strength [65]. Similar results have been obtained in the present study through MD simulations, which showed that fluoride tends to associate preferentially with calcium due to the higher ionic field strength of the latter, resulting in the formation of alkali/alkaline-earth rich ionic aggregates (CaF^{+} and, in lower amounts, Na-F) as has also been reported for fluoride containing silicate glasses [12, 30, 49]. The models highlight that only a minor fraction of fluoride ions are bonded to P for the compositions investigated, even though this P-bonded fraction appears to increase with the CaF_2 amount. Nonetheless, the preferential fluoride interaction for these glasses appears to involve the modifier cations. The ability of fluoride ions to strip modifier cations from the glass network induces re-polymerization in the glass structure, thus increasing the network connectivity and slowing down the rate of chemical dissolution. The MD simulation results in this respect are in good agreement with the structural data obtained from ^{31}P and ^{23}Na MAS-NMR spectroscopy, for which slight re-polymerization in glass structure is evident at higher fluoride content (Table 2). However, unlike the MD simulations, where influence of fluoride on the structure of glasses was evident starting from initial glass composition, in the experimental glasses these structural changes were apparent only at higher CaF_2 concentrations, probably due to the partial loss of fluoride from the glasses during melting. According to the literature, 5-23% CaF_2 is lost from fluoride-containing phosphosilicate glasses during melting [76]. While we could not obtain a similar reference data point for fluoride solubility/retention in phosphate glass melts, it has been shown that only 10% of the total chlorine content can be retained in iron phosphate glasses [77]. In the present study, we did observe a thin layer of white colored precipitates on the bottom part of the Pt-Rh lid (covering the Pt crucible) indicating the volatilization of fluorine. Therefore, fluorine loss in the present study cannot be

neglected. Although we could not ascertain the exact fluoride concentration in glasses for the present study, we are assuming it to be comparatively higher than that for chlorine (as observed in iron phosphate glasses [77]) as has been evidenced in the literature (mainly in silicate glasses) [27, 28, 78]. This assumption is also supported by our thermal analysis (decrease in crystallization temperature and change in the shape of crystallization curve with increasing fluoride content) and chemical dissolution results as discussed above.

With respect to the apatite forming ability and corrosion of glasses, fluoride incorporation in glasses slows down their chemical dissolution in DI water due to repolymerization of the phosphate glass network, but only until the stage where glass network structure is not broken by the attack of H^+ and molecular water. However, this increase in chemical durability does not seem to affect their apatite forming ability (in SBF) due to higher solubility (in comparison to silicate glasses) and congruent dissolution behavior of phosphate glasses.

When investigating the influence of pH on the dissolution of phosphate glasses, it has been experimentally shown by Bunker et al. [72] that at pH <6.5 (i.e. acidic media), phosphate glasses adsorb an excess of protons while at pH > 6.5 (neutral and basic media), excess of OH ions are adsorbed. Accordingly, in acidic media, phosphate chains are protonated due to ion exchange reactions between $Na^+ \leftrightarrow H^+$ at the beginning of the glass corrosion process, which disrupts the ionic crosslinks between phosphate chains. This allows water to penetrate into the glass faster, leading to rapid chain hydration and uniform dissolution. Therefore, we could not observe any significant impact of fluoride content on the dissolution of glasses in acidic media as is evident from Figure 11. However, in basic solutions, it seems that along with OH adsorption, there also exists an ion exchange reaction between $F^- \leftrightarrow OH^-$ leading to increase in weight gain with increasing fluoride content (as is evident from Figure 12). In-depth structural (for example,

secondary ion mass spectroscopy, double resonance NMR) and chemical dissolution studies on glass samples are required in order to validate this hypothesis.

Chapter 5

Conclusions and Future Work

The influence of fluoride on the structure and chemical dissolution behavior of phosphate-based bioactive glasses has been studied. The incorporation of fluoride ions in these glasses induces re-polymerization in the phosphate glass network by stripping the network modifying cations from the glass network. This leads to a slow down of the chemical dissolution of glasses, but only until the stage where the glass network structure is not broken by the attack of H^+ and molecular water. After this stage, phosphate glasses degrade congruently and fluoride content ceases to have an impact on chemical durability. Due to this reason, no significant influence of fluoride incorporation on the apatite-forming ability of these glasses was detected. Therefore, it appears possible to incorporate the beneficial properties of fluoride ions in phosphate-based bioactive glasses without any deterioration in their bioactivity. However, volatilization of fluoride from the glass melts needs to be studied further in order to to develop a better and precise understanding of structure-property relationships in these glasses. It is imperative that a more quantative relationship be developed between experimental results and molecular dynamic simulations. We have been able to define the trends associated with fluoride incorporation in sodalime phosphate based glass systems. We have also been able to corelate our experimental data to molecular structure well on the account of the information provided by MD simulations. However, the relative extent to which fluoride impacts the glass structure needs a more precise control over its incorporation. The effects observed in molecular simulations at small fluoride concentrations were only apperent at much higher concentrations in the experimentally fabricated glasses. In order to develop a completely linear agreement between the two results the efficiency of fluoride incorporation needs to be enhanced. Only then the role of fluoride in these glass systems can be fundamentally quantified.

Future research is also warranted on glasses with higher fluoride content, in order to clarify whether the structural trends highlighted here may change when sufficiently high fluoride amounts are incorporated in the glass system. DTA analysis of the glasses revealed a sudden rise in the T_g of sample F-10, suggesting a non linear increase in the structural connectivity. Moreover, the anomolous behavior of F-10 was also apperent in the normalized Na release profile in DI water. It took F-10 longer to achieveequilibrum with the dissolution medium compared to other glasses. These trends need to be well elucidated to create a general model of fluoride containing phosphate glass dissolution.

Chapter 6

Supplementary Results

The data and figures presented in the preceding chapters have directly led us to our conclusions regarding the impact of fluoride incorporation in soda-lime phosphate glasses. However, numerous other pieces of information were collected during the course of research. These results were instrumental in our analysis, but were not included in our submitted manuscript for publication on the account of space constraints. These results helped us zero down to the major parameters affecting our dissolution kinetics and eliminate any non-significant ones. Presented henceforth is a discussion of these results and our conclusions based on them.

6.1 Apatite forming ability of glasses in SBF

Glass dissolution in simulated body fluids did not make a substantial change in the pH of the solutions over time. Figure x presents the variation of pH with time for F-0, F-5 and F-10. The pH of the system remained almost constant between 7.3 and 7.4 for all the glasses. Unlike the DI water system where a significant drop in the pH was observed, the leached ions in this case did not create a major impact. The reason for this is that SBF is already saturated with similar ions and incorporation of moderate amounts of calcium, sodium and phosphates from the glasses is not sufficient to bring about a significant change in the solution pH. The relative concentrations of the various ions have already been discussed in the preceding chapters. It can be expected that the dissolution experiments lasting for more than 48 hours might leach sufficient ions into the solution, however the simulated body fluids need to be replaced after every 48 hours, hence no pH or dissolution data is available for these fluids post this dissolution time.

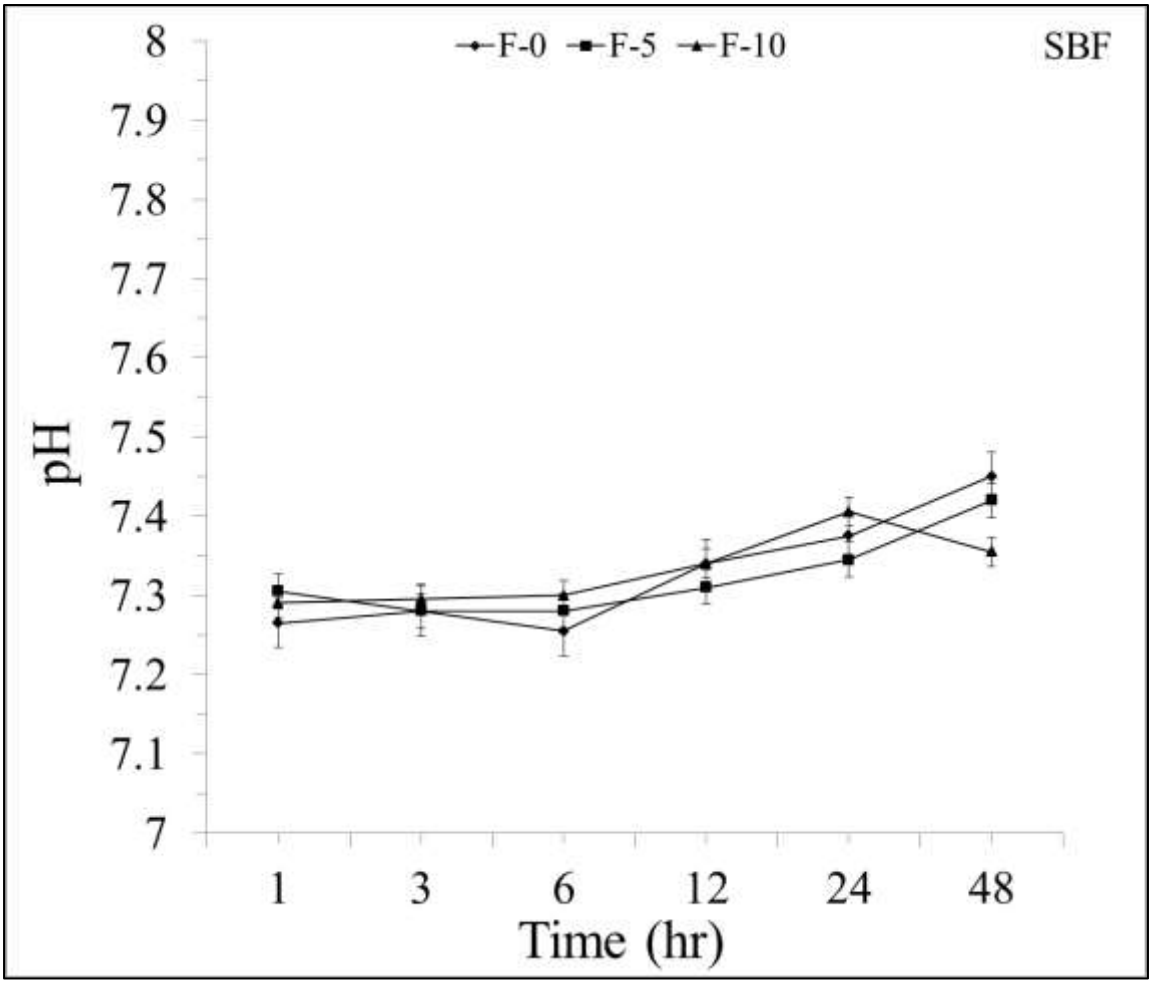


Figure 13 pH variation of SBF (with time) due to dissolution of glasses

Figure 7 (a) (b) and (c) present the normalized dissolution of phosphate, calcium and sodium ions as a function of time. As in the results section we did not find any significant impact of fluoride incorporation on the dissolution kinetics of these ions in the system. Congruency in the degradation of soda lime phosphate glasses is the key factor responsible for it. The $Na^{+} \leftrightarrow H^{+}$ ion exchange soda lime phosphate based glass systems is the rate determining step of dissolution. Fluoride ions as mentioned above slightly affect the initial dissolution rate of Na. However, step (2) dominates the phosphate and calcium dissolution which is largely un-affected by fluoride incorporation. After the initial 1 hour of dissolution the release rate of sodium fell almost to zero.

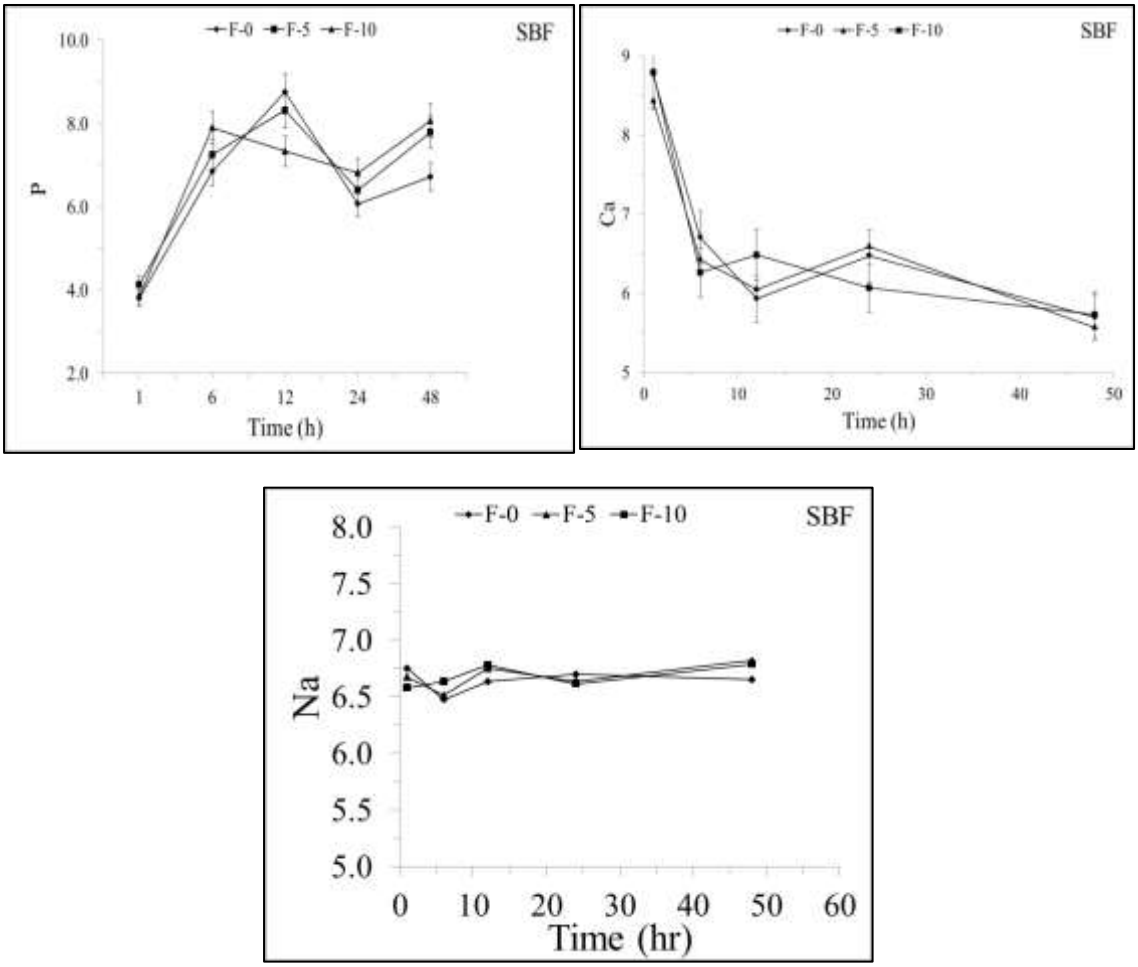


Figure 14 Normalized (b) phosphate and (c) calcium (d) sodium release rates from glass powders (with respect time) in F-0, F-5 and F-10 in SBF

6.2 Dissolution behavior of glasses in deionized water

Post the initial phase of dissolution i.e. step (1) where the $Na^{+} \leftrightarrow H^{+}$ ion exchange dominates, we could not see any substantial impact of fluoride incorporation on the dissolution kinetics of the glass system. Step (2) of the dissolution process occurs after the network has broken, which leads to congruent dissolution of all the components from the glass system. Figures 10 (b) and (c) presnet the dissolution of phosphate and calcium ions in DI water as a function of time. This step remains largely unaffected by fluoride incorporation. We can see that the system attains equilibrium within 50 hours of dissolution and and after that the concentration of the ions in the system remains constant. There is no net diffusion of ions from the glasses into the solution.

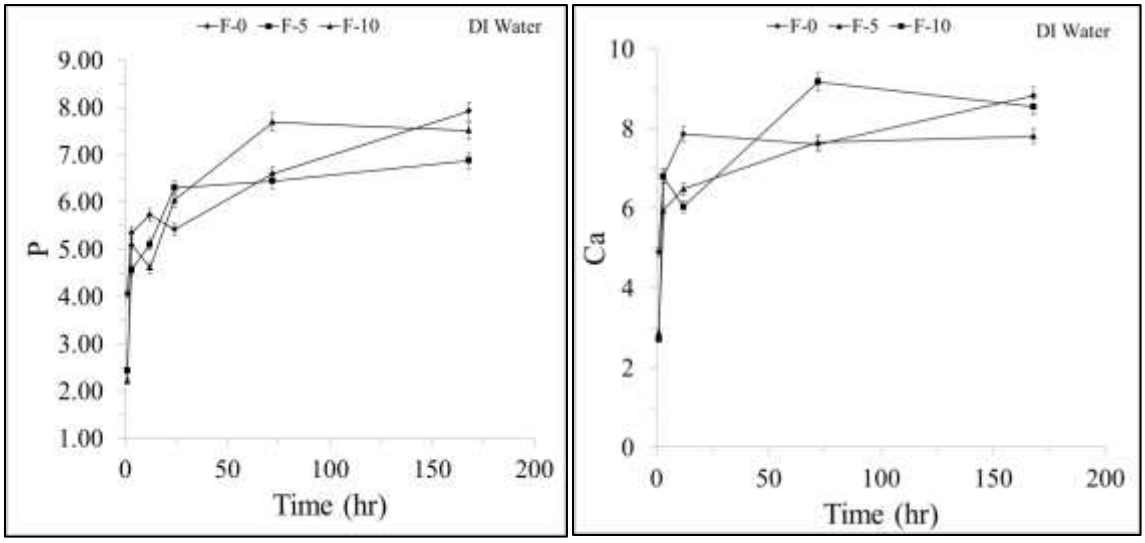


Figure 15 Normalized (b) phosphate and (c) calcium release rates from glass powders (with respect time) in F-0, F-5 and F-10 in DI water

6.3 Influence of pH on dissolution behavior of glasses

Figure 12 summarizes the imapct of pH over the dissolution behaviour of these glasses. The figure presents the weight loss of F-0, F-5 and F-7.5 as a function of pH of the system. As the pH increases the phosphate based glasses tend to absorb water from the dissolution medium and register an increase in weight as opposed to a loss. Figure y also suggests a deviation in the pH dependency of weight loss with the incorporation of fluoride in the system. As fluoride content increases in the glasses the system deviates towards a more linear relationship between the two parameters. Weight gain in fluoride free glasses increases more steeply as we move from a nuetral to a basic pH as opposed to the increase in the weight gain between acidic to nuetral conditions.

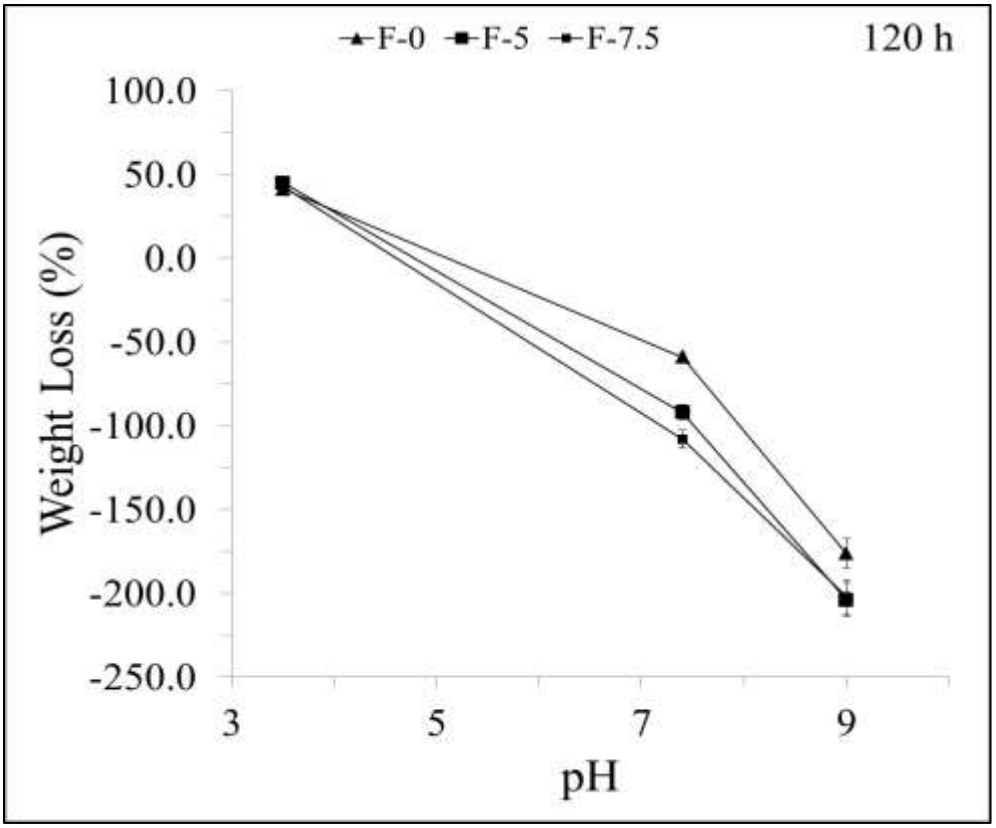


Figure 16 Variation of the weight loss behaviour with pH of the dissolution medium

References

[1] Hench, L. L. The Story of Bioglass. *J Mater Sci Mater Med* **2006**, *17*, 967–978.

[2] Hench, L. L. Glass and Genes: The 2001 W. E. S. Turner Memorial Lecture. *Glas. Technol.* **2003**, *44* (1), 1–10.

[3] Hench, L. L.; Polak, J. M. Third-Generation Biomedical Materials. *Sci.* **2002**, *295* (5557), 1014–1017.

[4] Jones, J. R. Review of Bioactive Glass: From Hench to Hybrids. *Acta Biomater.* **2013**, *9* (1), 4457–4486.

[5] Hench, L. L.; Day, D. E.; Höland, W.; Rheinberger, V. M. Glass and Medicine. *Int. J. Appl. Glas. Sci.* **2010**, *1* (1), 104–117.

[6] Hoppe, A.; Güldal, N. S.; Boccaccini, A. R. A Review of the Biological Response to Ionic Dissolution Products from Bioactive Glasses and Glass-Ceramics. *Biomaterials* **2011**, *32* (11), 2757–2774.

[7] Gorustovich, A. A.; Roether, J. A.; Boccaccini, A. R. Effect of Bioactive Glasses on Angiogenesis: A Review of In Vitro and In Vivo Evidences. *Tissue Eng. Part B Rev.* **2009**, *16* (2), 199–207.

[8] Tilocca, A. Current Challenges in Atomistic Simulations of Glasses for Biomedical Applications. *Phys. Chem. Chem. Phys.* **2014**, *16* (9), 3874–3880.

[9] Xynos, I. D.; Edgar, A. J.; Buttery, L. D. K.; Hench, L. L.; Polak, J. M. Gene-Expression Profiling of Human Osteoblasts Following Treatment with the Ionic Products of Bioglass® 45S5 Dissolution. *J. Biomed. Mater. Res.* **2001**, *55* (2), 151–157.

[10] Kapoor, S.; Goel, A.; Tilocca, A.; Dhuna, V.; Bhatia, G.; Dhuna, K.; Ferreira, J. M. F. Role of Glass Structure in Defining the Chemical Dissolution Behavior, Bioactivity and Antioxidant Properties of Zinc and Strontium Co-Doped Alkali-Free Phosphosilicate Glasses. *Acta Biomater.* **2014**, *10* (7), 3264–3278.

[11] Tilocca, A.; Cormack, A. N. Modeling the Water−Bioglass Interface by Ab Initio Molecular Dynamics Simulations. *ACS Appl. Mater. Interfaces* **2009**, *1* (6), 1324–1333.

[12] Goel, A.; Kapoor, S.; Tilocca, A.; Rajagopal, R. R.; Ferreira, J. M. F. Structural Role of Zinc in Biodegradation of Alkali-Free Bioactive Glasses. *J. Mater. Chem. B* **2013**, *1* (24), 3073–3082.

[13] Goel, A.; Rajagopal, R. R.; Ferreira, J. M. F. Influence of Strontium on Structure, Sintering and Biodegradation Behaviour of CaO–MgO–SrO–SiO2–P2O5–CaF2 Glasses. *Acta Biomater.* **2011**, *7* (11), 4071–4080.

[14] Bergandi, L.; Aina, V.; Garetto, S.; Malavasi, G.; Aldieri, E.; Laurenti, E.; Matera, L.; Morterra, C.; Ghigo, D. Fluoride-Containing Bioactive Glasses Inhibit Pentose Phosphate Oxidative Pathway and Glucose 6-Phosphate Dehydrogenase Activity in Human Osteoblasts. *Chem. Biol. Interact.* **2010**, *183* (3), 405–415.

[15] Brauer, D. S.; Karpukhina, N.; Law, R. V; Hill, R. G. Structure of Fluoride-Containing Bioactive Glasses. *J. Mater. Chem.* **2009**, *19* (31), 5629–5636.

[16] Ahmed, I.; Lewis, M.; Olsen, I.; Knowles, J. C. Phosphate Glasses for Tissue Engineering: Part 1. Processing and Characterisation of a Ternary-Based P2O5–CaO–Na_2O Glass System. *Biomaterials* **2004**, *25* (3), 491–499.

[17] Ahmed, I.; Lewis, M.; Olsen, I.; Knowles, J. C. Phosphate Glasses for Tissue Engineering: Part 2. Processing and Characterisation of a Ternary-Based P2O5–CaO–Na_2O Glass Fibre System. *Biomaterials* **2004**, *25* (3), 501–507.

[18] Franks, K.; Abrahams, I.; Knowles, J. C. Development of Soluble Glasses for Biomedical Use Part I: In Vitro Solubility Measurement. *J. Mater. Sci. Mater. Med.* **2000**, *11* (10), 609–614.

[19] Salih, V.; Franks, K.; James, M.; Hastings, G. W.; Knowles, J. C.; Olsen, I. Development of Soluble Glasses for Biomedical Use Part II: The Biological Response of Human Osteoblast Cell Lines to Phosphate-Based Soluble Glasses. *J. Mater. Sci. Mater. Med.* **2000**, *11* (10), 615–620.

[20] Bitar, M.; Salih, V.; Mudera, V.; Knowles, J. C.; Lewis, M. P. Soluble Phosphate Glasses: In Vitro Studies Using Human Cells of Hard and Soft Tissue Origin. *Biomaterials* **2004**, *25* (12), 2283–2292.

[21] Gough, J. E.; Christian, P.; Scotchford, C. A.; Rudd, C. D.; Jones, I. A. Synthesis, Degradation, and in Vitro Cell Responses of Sodium Phosphate Glasses for Craniofacial Bone Repair. *J. Biomed. Mater. Res.* **2002**, *59* (3), 481–489.

[22] Gough, J. E.; Christian, P.; Scotchford, C. A.; Jones, I. A. Long-Term Craniofacial Osteoblast Culture on a Sodium Phosphate and a Calcium/sodium Phosphate Glass. *J. Biomed. Mater. Res. A* **2003**, *66* (2), 233–240.

[23] Wiegand, A.; Buchalla, W.; Attin, T. Review on Fluoride-Releasing Restorative Materials--Fluoride Release and Uptake Characteristics, Antibacterial Activity and Influence on Caries Formation. *Dent. Mater.* **2007**, *23* (3), 343–362.

[24] Melo, M. A. S.; Morais, W. A.; Passos, V. F.; Lima, J. P. M.; Rodrigues, L. K. A. Fluoride Releasing and Enamel Demineralization around Orthodontic Brackets by Fluoride-Releasing Composite Containing Nanoparticles. *Clin. Oral Investig.* **2014**, *18* (4), 1343–1350.

[25] Petersson, L. G. The Role of Fluoride in the Preventive Management of Dentin Hypersensitivity and Root Caries. *Clin. Oral Investig.* **2013**, *17 Suppl 1*, S63–S71.

[26] Duncan, T. Study of Fluorine in Silicate Glass with ^{19}F Nuclear Magnetic Resonance Spectroscopy. *J. Appl. Phys.* **1986**, *60* (1), 130–136.

[27] Youngman, R. E.; Sen, S. Structural Role of Fluorine in Amorphous Silica. *J. Non. Cryst. Solids* **2004**, *349* (0), 10–15.

[28] Youngman, R. E.; Sen, S. The Nature of Fluorine in Amorphous Silica. *J. Non. Cryst. Solids* **2004**, *337* (2), 182–186.

[29] Hayakawa, S.; Ohtsuki, C.; Matsumoto, S.; Osaka, A.; Miura, Y. Molecular Dynamic Simulation of Heterogeneity and Chemical States of Fluorine in Amorphous Alkaline Earth Silicate Systems. *Comput. Mater. Sci.* **1998**, *9* (3–4), 337–342.

[30] Lusvardi, G.; Malavasi, G.; Cortada, M.; Menabue, L.; Menziani, M.C.; Pedone, A.; Segre, U. Elucidation of the Structural Role of Fluorine in Potentially Bioactive Glasses by Experimental and Computational Investigation. *J Phys Chem B* **2008**, *112*, 12730–12739.

[31] Brow, R. K.; Osborne, Z. A.; Kirkpatrick, R. J. A Multinuclear MAS NMR Study of the Short-Range Structure of Fluorophosphate Glass. *J. Mater. Res.* **1992**, *7* (07), 1892–1899.

[32] Brow, R. K.; Osborne, Z. A. XPS Studies of Fluorine Bonding in Phosphate Glasses. *Surf. Interface Anal.* **1996**, *24* (2), 91–94.

[33] Brow, R. K.; Phifer, C. C.; Xu, X. J.; Day, D. E. An X-Ray Photoelectron Spectroscopy Study of Anion Bonidng in tin(II) Fluorophosphate Glass. *Phys. Chem. Glas. 33* (2), 33–39.

[34] Kirkpatrick, R. J.; Brow, R. K. Nuclear Magnetic Resonance Investigation of the Structures of Phosphate and Phosphate-Containing Glasses: A Review. *Solid State Nucl. Magn. Reson.* **1995**, *5* (1), 9–21.

[35] Santos, L. F.; Almeida, R. M.; Tikhomirov, V. K.; Jha, A. Raman Spectra and Structure of Fluoroaluminophosphate Glasses. *J. Non. Cryst. Solids* **2001**, *284* (1–3), 43–48.

[36] Karmakar, B.; Kundu, P.; Dwivedi, R.N. UV Transparency and Structure of Fluorophosphate Glasses. *Mater. Lett.* **2002**, *57* (4), 953–958.

[37] Zhang, L.; de Araujo, C.C.; Hellmut, E. Structural Role of Fluoride in Aluminophosphate Sol-Gel Glasses: High-Resolution Double-Resonance NMR Studies . *J. Phys. Chem. B* **2007**, *111*, 10402– 10412.

[38] Christie, J. K.; Ainsworth, R. I.; de Leeuw, N. H. Ab Initio Molecular Dynamics Simulations of Structural Changes Associated with the Incorporation of Fluorine in Bioactive Phosphate Glasses. *Biomaterials* **2014**, *35* (24), 6164–6171.

[39] Amoureux, J.-P.; Fernandez, C.; Steuernagel, S. ZFiltering in MQMAS NMR. *J. Magn. Reson. Ser. A* **1996**, *123* (1), 116–118.

[40] Amoureux, J.; Huguenard, C.; Engelke, F.; Taulelle, F. Unified Representation of MQMAS and STMAS NMR of Half-Integer Quadrupolar Nuclei. *Chem. Phys. Lett.* **2002**, *356* (5), 497–504.

[41] Smith, W.; Forester, T. R. DL_POLY_2.0: A General-Purpose Parallel Molecular Dynamics Simulation Package. *J. Mol. Graph.* **1996**, *14* (3), 136–141.

[42] Tilocca, A. Models of Structure, Dynamics and Reactivity of Bioglasses: A Review. *J. Mater. Chem.* **2010**, *20* (33), 6848–6858.

[43] Tilocca, A. Molecular Dynamics Simulations of a Bioactive Glass Nanoparticle. *J. Mater. Chem.* **2011**, *21* (34), 12660–12667.

[44] Tilocca, A. Short- and Medium-Range Structure of Multicomponent Bioactive Glasses and Melts: An Assessment of the Performances of Shell-Model and Rigid-Ion Potentials. *J. Chem. Phys.* **2008**, *129* (8), 84504.

[45] Tilocca, A.; de Leeuw, N. H.; Cormack, A. N. Shell-Model Molecular Dynamics Calculations of Modified Silicate Glasses. *Phys. Rev. B* **2006**, *73* (10), 104209.

[46] Tilocca, A.; Cormack, A. N.; de Leeuw, N. H. The Structure of Bioactive Silicate Glasses: New Insight from Molecular Dynamics Simulations. *Chem. Mater.* **2007**, *19* (1), 95–103.

[47] Tilocca, A.; Cormack, A. N.; de Leeuw, N. H. The Formation of Nanoscale Structures in Soluble Phosphosilicate Glasses for Biomedical Applications: MD Simulations. *Faraday Discuss.* **2007**, *136*, 23–45.

[48] Carta, D.; Pickup, D. M.; Knowles, J. C.; Ahmed, I.; Smith, M. E.; Newport, R. J. A Structural Study of Sol–gel and Melt-Quenched Phosphate-Based Glasses. *J. Non. Cryst. Solids* **2007**, *353* (18–21), 1759–1765.

[49] Lusvardi, G.; Malavasi, G.; Tarsitano, F.; Menabue, L.; Menziani, M. C.; Pedone, A. Quantitative Structure-Property Relationships of Potentially Bioactive Fluoro Phospho-Silicate Glasses. *J. Phys. Chem. B* **2009**, *113* (30), 10331–10338.

[50] Tilocca, A. Cooling Rate and Size Effects on the Medium-Range Structure of Multicomponent Oxide Glasses Simulated by Molecular Dynamics. *J. Chem. Phys.* **2013**, *139* (11), 114501.

[51] Tas, A. C. Synthesis of Biomimetic Ca-Hydroxyapatite Powders at 37 Degrees C in Synthetic Body Fluids. *Biomaterials* **2000**, *21* (14), 1429–1438.

[52] Hrubý, A. Evaluation of Glass-Forming Tendency by Means of DTA. *Czechoslov. J. Phys. B* **1972**, *22* (11), 1187–1193.

[53] Christie, J. K.; Pedone, A.; Menziani, M. C.; Tilocca, A. Fluorine Environment in Bioactive Glasses: Ab Initio Molecular Dynamics Simulations. *J. Phys. Chem. B* **2011**, *115* (9), 2038–2045.

[54] Pedone, A.; Charpentier, T.; Menziani, M. C. The Structure of Fluoride-Containing Bioactive Glasses: New Insights from First-Principles Calculations and Solid State NMR Spectroscopy. *J. Mater. Chem.* **2012**, *22* (25), 12599–12608.

[55] Ainsworth, R. I.; Tommaso, D. Di; Christie, J. K.; de Leeuw, N. H. Polarizable Force Field Development and Molecular Dynamics Study of Phosphate-Based Glasses. *J. Chem. Phys.* **2012**, *137* (23), -.

[56] Ilieva, D.; Jivov, B.; Bogachev, G.; Petkov, C.; Penkov, I.; Dimitriev, Y. Infrared and Raman Spectra of Ga2O3–P2O5 Glasses. *J. Non. Cryst. Solids* **2001**, *283* (1–3), 195–202.

[57] Shih, P. Y.; Yung, S. W.; Chin, T. S. FTIR and XPS Studies of P2O5–Na2O–CuO Glasses. *J. Non. Cryst. Solids* **1999**, *244* (2–3), 211–222.

[58] Lemos, A. F.; Rocha, J. H. G.; Quaresma, S. S. F.; Kannan, S.; Oktar, F. N.; Agathopoulos, S.; Ferreira, J. M. F. Hydroxyapatite Nano-Powders Produced Hydrothermally from Nacreous Material. *J. Eur. Ceram. Soc.* **2006**, *26* (16), 3639–3646.

[59] Landi, E.; Celotti, G.; Logroscino, G.; Tampieri, A. Carbonated Hydroxyapatite as Bone Substitute. *J. Eur. Ceram. Soc.* **2003**, *23* (15), 2931–2937.

[60] Alder, H. H.; Kerr, P. F. Infrared Study Of Aragonite and Calcite. *Am. Mineral.* **1962**, *47*, 700–717.

[61] Rey, C.; Collins, B.; Goehl, T.; Dickson, I. R.; Glimcher, M. J. The Carbonate Environment in Bone Mineral: A Resolution-Enhanced Fourier Transform Infrared Spectroscopy Study. *Calcif. Tissue Int.* **1989**, *45* (3), 157–164.

[62] Gao, H.; Tan, T.; Wang, D. Dissolution Mechanism and Release Kinetics of Phosphate Controlled Release Glasses in Aqueous Medium. *J. Control. Release* **2004**, *96* (1), 29–36.

[63] Massera, J.; Bourhis, K.; Petit, L.; Couzi, M.; Hupa, L.; Hupa, M.; Videau, J. J.; Cardinal, T. Effect of the Glass Composition on the Chemical Durability of Zinc-Phosphate-Based Glasses in Aqueous Solutions. *J. Phys. Chem. Solids* **2013**, *74* (1), 121–127.

[64] Dohler, F.; Mandlule, A.; van Wullen, L.; Friedrich, M.; Brauer, D. S. 31P NMR Characterisation of Phosphate Fragments during Dissolution of Calcium Sodium Phosphate Glasses. *J. Mater. Chem. B* **2015**, *3* (6), 1125–1134.

[65] Christie, J. K.; Ainsworth, R. I.; Di Tommaso, D.; de Leeuw, N. H. Nanoscale Chains Control the Solubility of Phosphate Glasses for Biomedical Applications. *J. Phys. Chem. B* **2013**, *117* (36), 10652–10657.

[66] Christie, J. K.; Tilocca, A. Integrating Biological Activity into Radioisotope Vectors: Molecular Dynamics Models of Yttrium-Doped Bioactive Glasses. *J. Mater. Chem.* **2012**, *22* (24), 12023– 12031.

[67] Kansal, I.; Goel, A.; Tulyaganov, D. U.; Santos, L. F.; Ferreira, J. M. F. Structure, Surface Reactivity and Physico-Chemical Degradation of Fluoride Containing Phospho-Silicate Glasses. *J. Mater. Chem.* **2011**, *21* (22), 8074–8084.

[68] Lusvardi, G.; Malavasi, G.; Menabue, L.; Aina, V.; Morterra, C. Fluoride-Containing Bioactive Glasses: Surface Reactivity in Simulated Body Fluids Solutions. *Acta Biomater.* **2009**, *5* (9), 3548–3562.

[69] Brauer, D. S.; Karpukhina, N.; O'Donnell, M. D.; Law, R. V; Hill, R. G. Fluoride-Containing Bioactive Glasses: Effect of Glass Design and Structure on Degradation, pH and Apatite Formation in Simulated Body Fluid. *Acta Biomater.* **2010**, *6* (8), 3275–3282.

[70] Ogino, M.; Ohuchi, F.; Hench, L. L. Compositional Dependence of the Formation of Calcium Phosphate Films on Bioglass. *J. Biomed. Mater. Res.* **1980**, *14* (1), 55–64.

[71] Khor, S. F.; Talib, Z. A.; Daud, W. M.; Sidek, H. A. A. Degradation Study on Ternary Zinc Magnesium Phosphate Glasses. *J. Mater. Sci.* **2011**, *46* (24), 7895–7900.

[72] Bunker, B. C.; Arnold, G. W.; Wilder, J. A. Phosphate Glass Dissolution in Aqueous Solutions. *J. Non. Cryst. Solids* **1984**, *64* (3), 291–316.

[73] Christie, J. K.; Ainsworth, R. I.; de Leeuw, N. H. Investigating Structural Features Which Control the Dissolution of Bioactive Phosphate Glasses: Beyond the Network Connectivity. *J. Non. Cryst. Solids* No. 0.

[74] Abou Neel, E.A.; Pickup, D.M.; Valappil, S.P.; Newport, R. J.; Knowles, J. C. Bioactive Functional Materials: A Perspective on Phosphate-Based Glasses. *J. Mater. Chem.* **2009**, *19*, 690–701.

[75] Pickup, D. M.; Ahmed, I.; Knowles, J. C.; Smith, M. E.; Newport, R. J. The Structure of Phosphate Glass Biomaterials from Neutron Diffraction and 31 P Nuclear Magnetic Resonance Data. *J. Phys. Condens. Matter* **2007**, *19* (41), 415116.

[76] Brauer, D. S.; Mneimne, M.; Hill, R. G. Fluoride-Containing Bioactive Glasses: Fluoride Loss during Melting and Ion Release in Tris Buffer Solution. *J. Non. Cryst. Solids* **2011**, *357* (18), 3328–3333.

[77] Mesko, M. G.; Day, D. E.; Bunker, B. C. Immobilization of CsCl and SrF2 in Iron Phosphate Glass. *Waste Manag.* **2000**, *20* (4), 271–278.

[78] Hermann, W.; Rau, H.; Ungelenk, J. Solubility and Diffusion of Chlorine in Silica Glass. *Berichte der Bunsengesellschaft für Phys. Chemie* **1985**, *89* (4), 423–426.